

Chapter1- Introduction to Optical Coherence Tomography

**Fedra Hajizadeh [corresponding author] (MD. Noor Ophthalmology Research Center, Noor Eye Hospital, No. 96, Esfandiar Blvd., Vali'asr Ave., Tehran, Iran; Tel: +98 21 82400, Fax: +98 2188650 501; e-mail:fedra_hajizadeh@yahoo.com; fhajizadeh@noorvision.com)*

** Rahele Kafieh (Medical Image and Signal Processing Research Center, School of Advanced Technologies in Medicine, Isfahan University of Medical Sciences, Isfahan, Iran; Biosciences Institute, Newcastle University, Newcastle upon Tyne, UK, email: Rkafieh@amt.mui.ac.ir)*

** M. Tajmirriahi (Medical Image and Signal Processing Research Center, School of Advanced Technologies in Medicine, Isfahan University of Medical Sciences, Isfahan, Iran e-mail: mtrahi2000@amt.mui.ac.ir)*

Abstract

(1) Basics and principles of optical coherence tomography (OCT), which briefly discuss the mechanisms and operation of OCT systems and a comparison of old and new systems (time domain vs. spectral domain) and their reproducibility. It concisely explains the frequency domain OCT, multiple reference OCT and hand held. (2) Normal OCT, which describes normal findings and variations that are expected on normal OCT images, and the layers of the normal retina and in different parts of the posterior segment. (3) Anterior segment OCT, which

describe the mechanism and clinical applications in various disease (4) Enhanced-depth imaging (EDI)-OCT and its applications and indications in various diseases such as choroidal tumors, age-related macular degeneration, diabetic retinopathy, central serous chorioretinopathy, glaucoma, intraocular inflammation, and myopia. Moreover, choroidal measurement and its variations under different conditions are discussed. (5) OCT angiography, which explains the mechanism and Clinical application and limitations of OCTA (6) Limitations and indications of OCT, which evaluate and explain the drawbacks and advantages of this diagnostic method for the exploration of ocular pathologies. (7) Pitfalls and artifacts, which covers and illustrates diagnostic pitfalls and artifacts in OCT image interpretation in circumstances such as the presence of an epiretinal membrane and myopia (8)

Artificial intelligence in OCT image analysis, which describes the classification and image synthesis and enhancement.

Keywords

Optical coherence tomography, Enhanced depth imaging, Artificial intelligence, Optical coherence angiography

I-Basic Principles of Optical Coherence Tomography

Introduction to Optical Coherence Tomography

similar to that of ultrasound image acquisition, except that OCT uses light beams in place of sound profiles. Comparable to ultrasound, each A-scan signal is acquired through axial reflectance from various layers of an object. The location of internal layers can be determined by using the signal-echo delay times of each structure. The collection of cross-sectional A-scans creates the B-scan or cross-sectional image. Unlike in ultrasound imaging, there is no need for direct contact with the eye to transmit or receive light signals. In addition, higher spatial resolution can be achieved by using light instead of ultrasound waves [1]. Optical coherence tomography achieves a resolution of a few micrometers by using different light resources such as super luminescent diodes, ultrashort-pulsed lasers, or supercontinuum lasers. This method can have many applications in the imaging of anatomical structures. Information concerning the internal layers of medical structures is of interest to scientists. An important feature of an imaged object is the maximum allowable depth of 1–2 millimeters for which OCT is applicable. At greater depths, the scattered beam will be too weak to be processed for image reconstruction. Figure 1.1 depicts a block-diagram of this imaging technique.

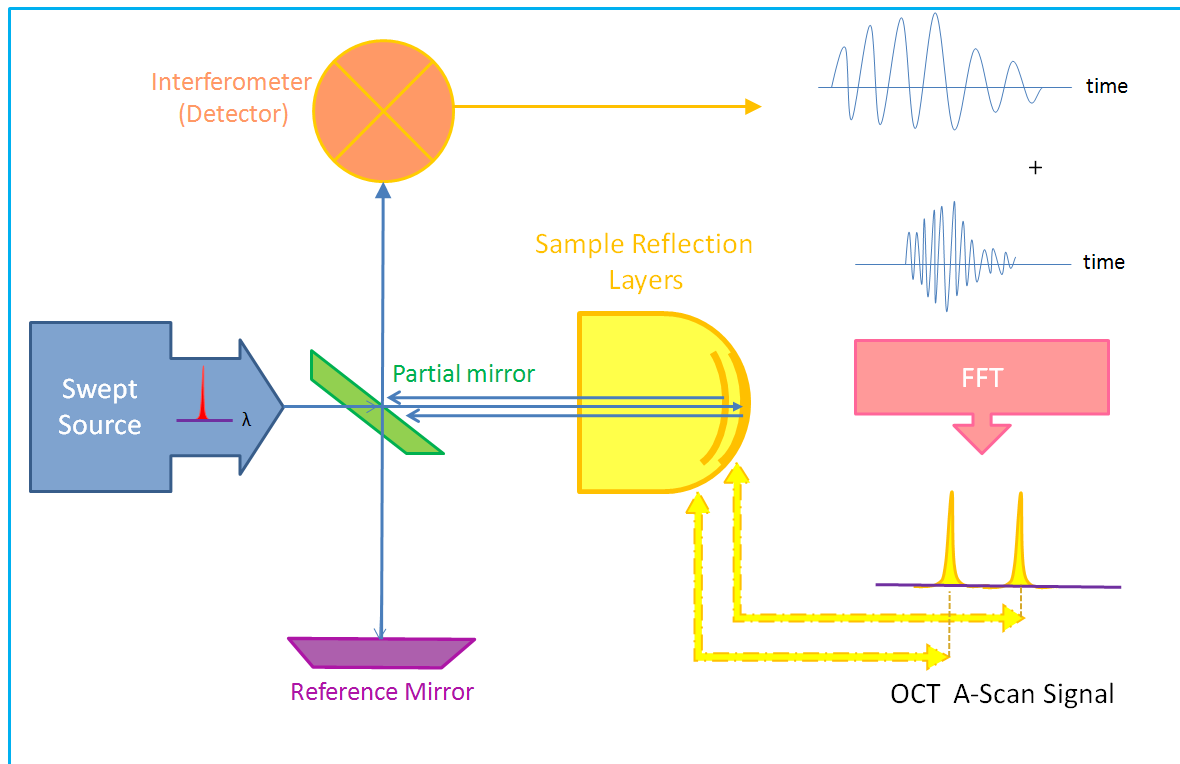


Fig.1. 1 Block diagram of optical coherence tomography
FFT fast Fourier transform, *OCT* optical coherence tomography

Principles of Optical Coherence Tomography

In vivo OCT imaging of the anterior section of the eye with approximately 10- μ m resolution was first reported in 1994 [2]. Working with two different teams, Hee and colleagues [2], [3] introduced OCT of the human retina to discriminate between different layers of the retina, morphological content of the fovea and optic disc, and thickness of the retinal nerve fiber layer. Table 1.1 illustrates the comparison of available commercial OCT Systems and their specifications which will be described in this section.

Table 1.1 Comparison of Optical Coherence Tomography Systems

Company	Device	Technology	Wavelength, nm	Scan rate, KHz	Axial resolution, μm	Scan depth, mm	Scan width, mm
Zeiss	Visante	TD-OCT	1310	2	18	6	16
Heidelberg	SL-OCT	TD-OCT	1310	0.2	< 25	7	15
Zeiss	Cirrus	SD-OCT	840	27	5	5.8	3
Heidelberg	Spectralis	SD-OCT	870	40	7	1.8	9

Optovue	iVue	SD-OCT	840	26	5	2.3	13
Nidek	RS 3000	SD-OCT	880	53	7	2.1	9
Casia	SS1000	SS-OCT	1310	30	< 10	6	16
Topcon	Triton	SS-OCT	1050	100	8	3	12

Time Domain OCT

Optical coherence tomography uses interferometry in low-coherence or white light and creates cross-sectional images by using the difference between the reflected light from a biological tissue and the reference light beam. The incident light encountering a tissue may be scattered, transmitted, or absorbed.

According to principles of interferometry, the light from a light source reaches a beam splitter and is divided into two parts. One beam is the reference beam and the other beam passes through the imaged structure. Different boundaries inside the structure reflect this beam and the echo beams backscatter from each layer at different axial distances. At the same time this process is occurring, the reference beam is reflected from a mirror placed at a specific distance. The two beams are then combined again by an optical beam splitter and are sent to an optical detector. When the two beams match, constructive interference occurs.

In time domain OCT (TD-OCT), the aforementioned reference arm should be positioned mechanically to determine the matched distance (refer to Figure 1.2). Based on the autocorrelation property in a symmetric and low-coherence interferometer, the highest value of the envelope of this modulation can occur with matched path lengths.

For two partially coherent beams, the interference is achieved by the formula

$$I = k_1 I_s + k_2 I_s + 2\sqrt{(k_1 I_s) \cdot (k_2 I_s)} \cdot \text{Re}[\gamma(\tau)] \quad (1)$$

in which $I_s I_s$ is the source intensity, and $k_1 + k_2 < 1$ is the splitting ratio of the interferometer, and $\gamma(\tau)$ is the degree of coherence (i.e., the complex degree of coherence). The interference envelop depends on the time delay τ in signal achievement (i.e., the desired variable in OCT). Because of the gating issue in OCT, the complex degree of coherence is usually represented by a Gaussian model:

$$\gamma(\tau) = \exp \left[- \left(\frac{\pi \Delta \nu \tau}{2 \sqrt{\ln 2}} \right)^2 \right] \cdot \exp(-j2\pi \nu_0 \tau) \quad (2)$$

in which $\Delta \nu$ is the spectral bandwidth of the source in the frequency domain, and ν_0 is the central frequency of the source. In Eq. 2, an optical carrier modulates the envelope of the amplitude and the peak of the envelope for this modulation is placed at the desired distance from the object; its peak corresponds to surface reflectivity. Based on the Doppler phenomenon caused by the moving arm, an optical carrier would result. The frequency of the carrier is directly correlated with the speed of movement in the arm. Therefore, two functions can be defined for the moving arm: (1) depth scanning and (2) optical carrier with Doppler shift. In OCT, the frequency of the aforementioned optical carrier can be calculated by the formula

$$f_{\text{Dopp}} = \frac{2 \cdot \nu_0 \cdot u_s}{c} f_{\text{Dopp}} = \frac{2 \cdot \nu_0 \cdot u_s}{c} \quad (3)$$

in which ν_0 is the central frequency of the source, u_s is the movement speed of the arm, and c is the speed of light. Furthermore, the axial resolution of OCT is defined by the formula:

$$l_c = \frac{2 \ln 2}{\pi} \cdot \frac{\lambda_0^2}{\Delta \lambda} \approx 0.44 \cdot \frac{\lambda_0^2}{\Delta \lambda} \quad (4)$$

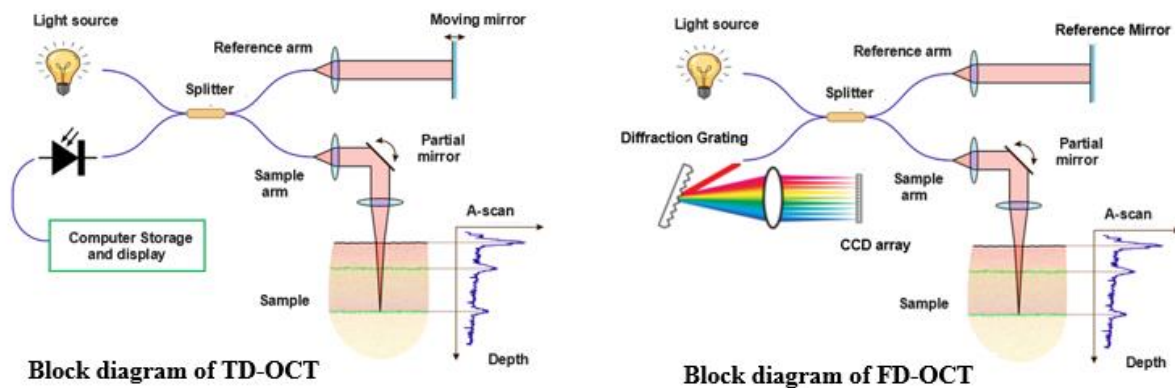


Fig.1. 2 Block diagram of time-domain OCT (TD-OCT) and frequency-domain OCT (FD-OCT).

Frequency Domain OCT

In frequency domain OCT, the movement of the arm is eliminated and, because of Fourier transform, depth information can be retrieved (Figure 1.1). In such systems, the speed is improved to more than 25,000 axial scans per second. This is faster than time domain detection [4]. Frequency domain OCT can be categorized into two subclasses: (1) spatially encoded and (2) time-encoded.

In spatially encoded frequency domain OCT (also called spectral domain OCT or Fourier domain OCT), the information can be retrieved by spreading different optical frequencies on an array of detectors (refer to Figure 1.2). Therefore, a single exposure would be sufficient to acquire the needed whole frequencies. However, the signal-to-noise (SNR) ratio is low because of the lower dynamic range of banding detectors, compared to that of single photosensitive diodes. Furthermore, the array of detectors does not distribute the frequency of the light equally on the detectors, which can also reduce the signal to noise ratio (SNR) in the reconstruction stage.

In time encoded frequency domain OCT (also called swept-source OCT), the information encoding is not based on frequencies; the time separation is instead replaced (refer to Figure 1.1). The spectrum is generated in single frequencies and reconstructed before the Fourier transform. The optical setup is easier than the previous method and the SNR increases. However, the nonlinear wavelength and high sensitivity are disadvantages of this strategy.

Multiple-reference OCT

Multiple-reference OCT (MR-OCT) [5] is based on conventional TD-OCT technology except the placement of the partial mirror which is very close to the reference mirror (see Figure 1). This causes multiple reflections of light between partial and the reference mirror. At each reflection, partial mirror transmits a small portion of light to the beam splitter as the reference light and reflects back the remaining portion to the reference mirror for successive reflections. The delay of each reflection between the partial and reference mirrors, caused by the round trip time between the two mirrors, produces interference signals corresponding to backscattered light from deeper regions within the target. The center points of the successive scan regions has the same distance between the partial mirror and the reference mirror. In this way, MR-OCT can scan multiple segments of a target from

surface to depth. MR-OCT has a solid-state design, which is low cost and robust. This technology can be used for use in targets with high volumes, and difficult operating environments.

Handheld OCT

Commercially available OCT systems are bulky in size, which limits their portability, but the most significant limitation of their using is their high cost [6]. Several studies have been done to implement small and portable OCT systems with handheld scanners to reduce the cost of OCT components. A primary handheld OCT probe was consisted of a pair of galvanometer-mounted mirrors for scanning. It was rather improved by including the use of a micro-electromechanical (MEMS) mirror for scanning, instead of the traditional use of galvanometers, and minimizing components within the handheld scanner [7], [8] . However, these systems have limited usage for point of care applications due to their bulky and expensive engines (the light source, spectrometer, PC, and interferometer optics). Recent works tries to use inexpensive components to develop a fully packaged silicon photonic integrated swept-source OCT to design miniaturized, low-cost, handheld linear OCT systems [9], [10]. However, these low-cost, portable systems can suffer from reduced imaging depth and signal to noise ratio (SNR). Therefore, design and implementation of a low-cost, portable OCT system needs more development to meet the required criteria for clinical retinal imaging.

Image Construction

B-scans can be obtained by consecutive axial scans at crosswise locations [1]. In most OCT images, the intensity of the backscattered signal is represented by false colors, in which white and red represent the highest intensity reflection and blue and black represent the lowest intensity. Figure 1.3 demonstrate the A-scan, B-scan, and volumetric data which can be obtained from OCT device. It can be seen that by putting the A-scan signals together and assigning a gray-level intensity to the amplitude of the signal in each time, the B-scan image is constructed.

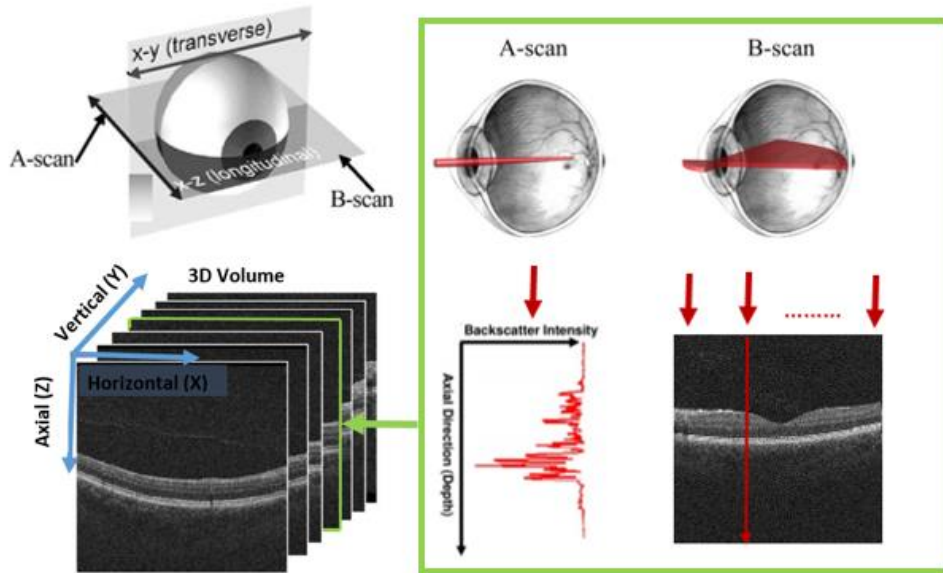


Fig.1. 3 Illustration of how to obtain A-scan, B-scan and 3D data by OCT system.

Reproducibility

The reproducibility between time domain OCT and frequency domain OCT has been compared in many studies[11]–[13] and intraclass correlation coefficients have been used to measure interscan reproducibility. Both imaging methods show a high degree of reproducibility.

II-Normal OCT

Diagnosis and treatment have been revolutionized with the advent of OCT retinal imaging [2],[14]. This is partly related to a very low axial resolution and to image acquisition and processing techniques (e.g., eye tracking and image averaging). A new version of this imaging modality has recently been introduced and can define choroidal structures in a way that previous techniques such as ultrasound and indocyanine green (ICG) angiography could not.

Optical coherence tomography has routinely been used in outpatient settings and is an important diagnostic tool for clinical decision-making. The use of intraoperative OCT has recently been introduced and is helpful in vitrectomy surgeries such as peeling of the ILM in a macular hole [15],[16] . Figure 1.4 is an OCT image of the normal macular structure.

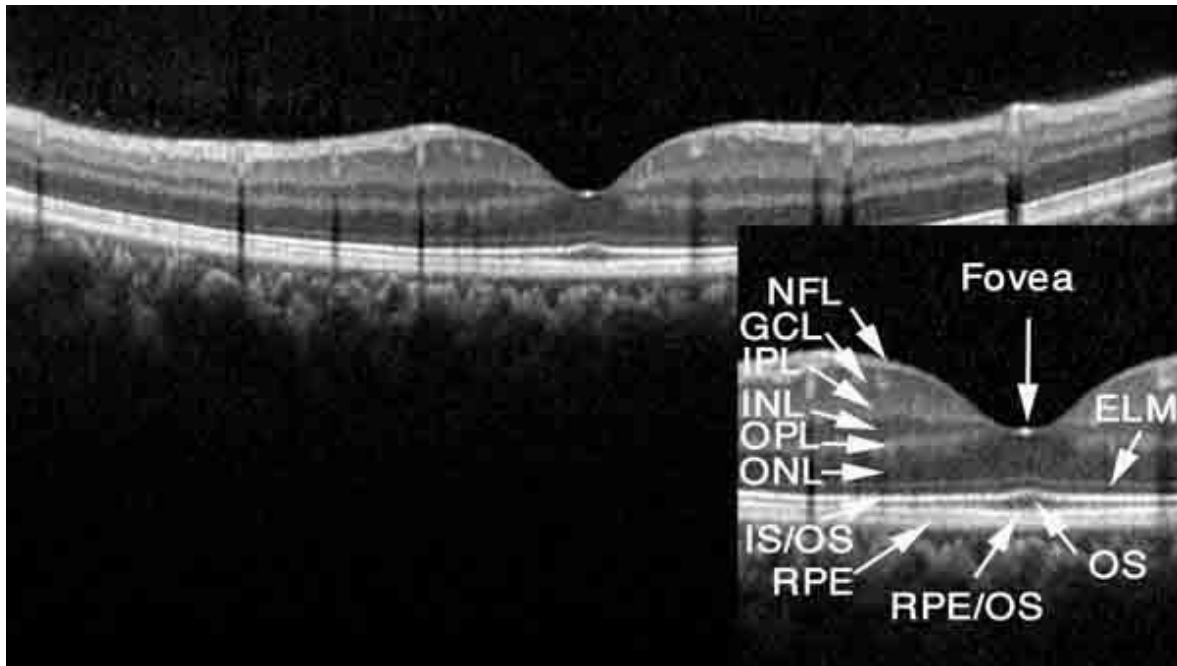


Fig.1. 4 A normal macula. The layers of the fovea are visible
ELM external limiting membrane, *GCL* ganglion cell layer, *INL* inner nuclear layer, *IPL* inner plexiform layer, *IS/OS* inner segment/outer segment interface (i.e., ellipsoid zone), *NFL* nerve fiber layer, *ONL* outer nuclear layer, *OPL* outer plexiform layer, *RPE* retinal pigment epithelium, *OS* outer segment, *RPE/OS* retinal pigment epithelium/outer segment interface (i.e., interdigitation zone)

The definition and attribution of the retinal layer, as illustrated by OCT, has changed in recent years. There is much debate pertaining to the four hyperreflective outer retinal bands detected with the current generation of OCT. Spaide et al. [17] recently reviewed the literature regarding the histology of the outer retina and used the data to create a scale model drawing. On the basis of their results, the first innermost layer is the external limiting membrane (i.e., the junctional complexes between the Muller cells and the photoreceptors [indicated by “a” in Fig.1.5]), the second layer is the ellipsoid portion of the inner segment (“b” in Fig.1.5), and the third layer is the interdigitation between the cone outer segments and the apical process of the retinal pigment epithelium in the contact cylinder (“d” in Fig.1.5). In the parafoveal region (1.5 mm from the foveal center), another band is added to this complex (i.e., between the second and third layer [“c” in Fig.1.5]) and is called the cone outer segment tip (COST).

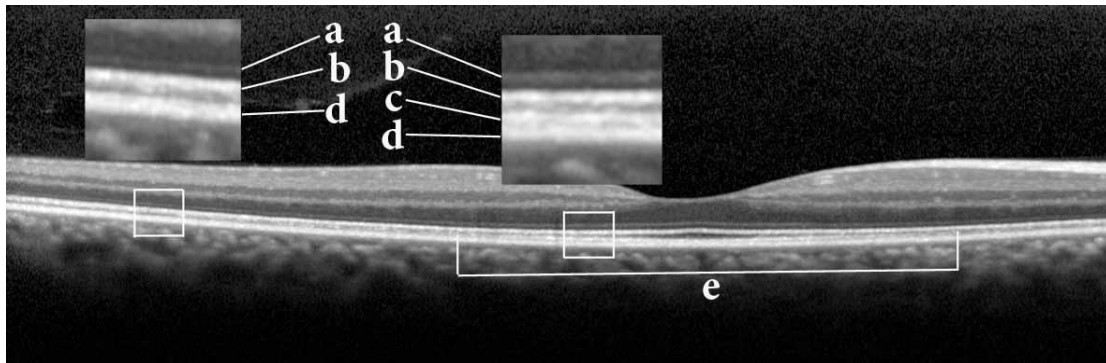


Fig.1. 5 Band “a” indicates the external limiting membrane, which is the junctional complex between the Muller cells and the photoreceptors. Band “b” corresponds to the ellipsoid section of the inner segment of the photoreceptors. Band “c” constitutes the contact region of the outer segment of cone photoreceptors with the cylindrical region or cone outer segment tip or interdigitation zone. This layer is detected in the fovea and parafoveal region (*e*), which contain predominantly cone photoreceptors. Band “d”, the outer band, represents the retinal pigment epithelium, which cannot be separated from the underlying Bruch’s membrane

The foveal outer segment pigment epithelium thickness (FOSPET) (Fig. 1.6) is another parameter that is defined as the distance between the outer borders of retinal pigment epithelium (RPE) and the inner border of hyperreflective photoreceptor inner segment/outer segment junction. The FOSPET should be measured at the thinnest point of the fovea. Witkin et al. [18] introduced the FOSPET as an indicator for quantifying photoreceptor loss in patients with retinitis pigmentosa.

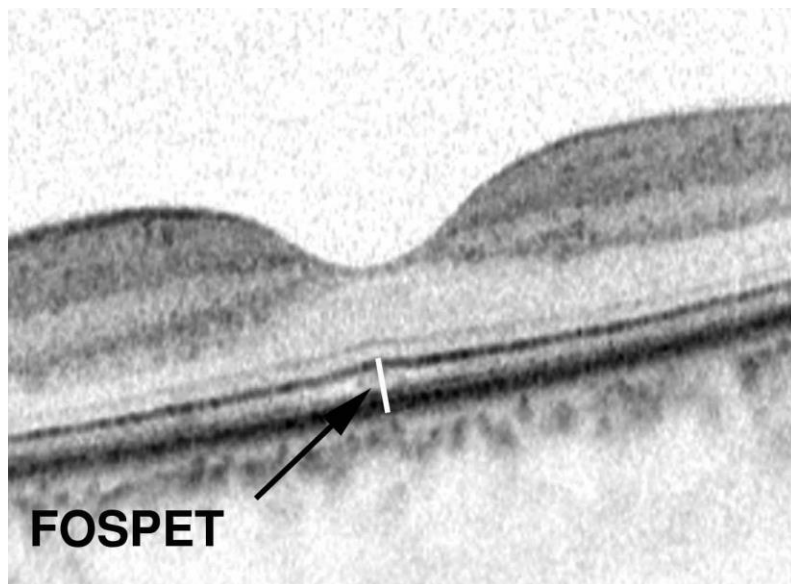


Fig.1. 6 The red line represents the foveal outer segment pigment epithelium thickness (FOSPET), which lies between the outer border of retinal pigment epithelium and the inner border of the

hyperreflective photoreceptor inner/outer segment junction. It is an indicator of cone photoreceptor health and visual acuity

Normal Macular Topographic Map

The topographic printout and schedule differ across different OCT devices, but a colorful image can usually be obtained with an Early Treatment Diabetic Retinopathy Study circle (1 mm, 3 mm, and 6 mm in diameter) at the center of the fovea (Fig 1.7) where each circle is segmented into four quadrants (i.e., superior, inferior, nasal, and temporal) [19].

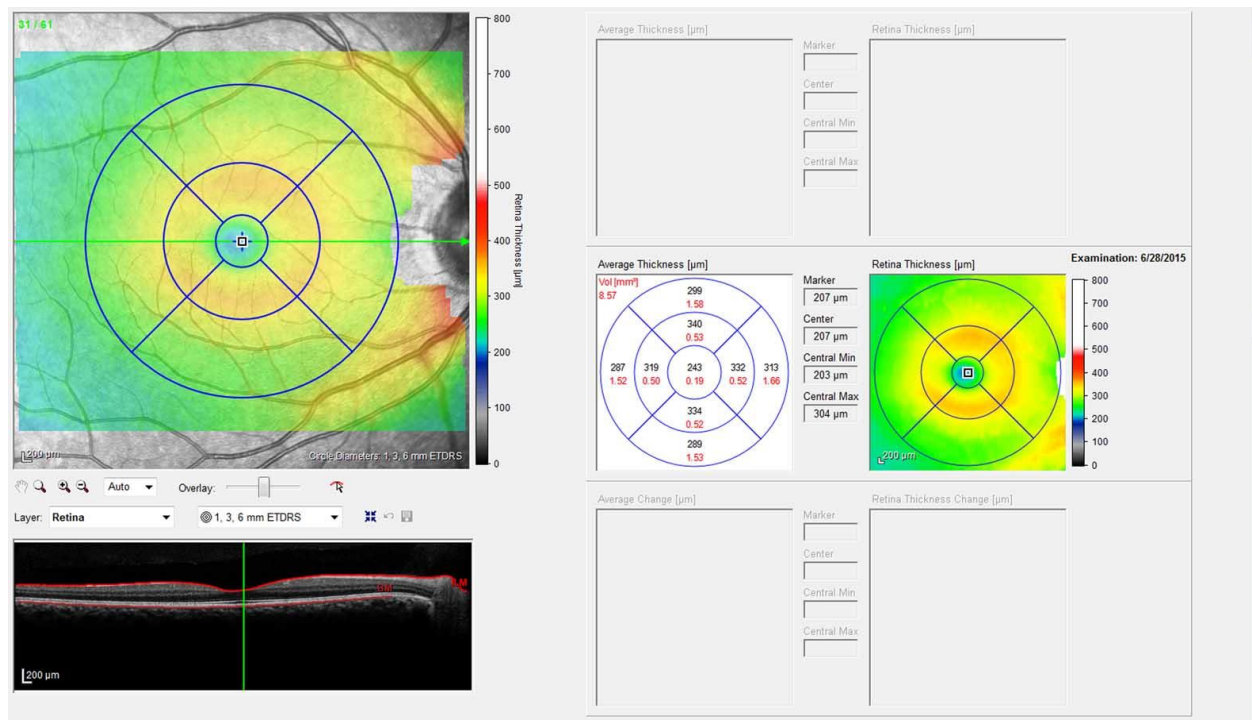


Fig.1. 7 A normal topographic map. The nasal quadrant is normally thicker than the other parts. The central fovea and central subfield are the thinnest part

The normal amount of retinal thickness is variable across different devices. This difference is related to the definition of retinal layer used by the OCT apparatus and segmentation algorithms. In time domain OCT devices such as the Stratus OCT (Carl Zeiss Meditec, Inc., Dublin, CA, USA), segmentation is based on the hyperreflective band, which corresponds to the inner segment/outer segment (IS/OS) junction area. However, in newer OCT devices using Fourier domain technology

measurements, the RPE layer is the outer boundary [20], [21]. The distance between the RPE layer and the IS/OS junction is approximately 34.7 μm . Therefore, newer devices may provide a larger number of retinal thickness measurements. The reproducibility of thickness measurements by an OCT apparatus depends on image registration and eye tracking options. The Spectralis OCT device (Heidelberg Engineering, Heidelberg, Germany) is superior because of its increased reproducibility in normal and pathologic conditions [22].

The measurement of macular thickness has greatly improved and is more reliable with better technology, decreased image acquisition time, increased number of scans per second, and greater resolution with better segmentation capability. The Cirrus HDOCT apparatus (Carl Zeiss Meditec, Inc.) measures macular thickness in nine macular subfields by 43.7–61.1 μm more than the Stratus CT apparatus (Carl Zeiss Meditec, Inc.) [23]. The Topcon 3D OCT-1000 (Tokyo, Japan) also measures the average macular thickness and the foveal central subfield by 33.9 μm and 21.3 μm , respectively, more than the Stratus CT [24]. Table 1.2 illustrates the differences in the measurement amounts among various OCT apparatuses.

Table 1.2 Macular thickness measurements

OCT apparatus	Foveal central point thickness (μm)	Average macular thickness (μm)	Macular volume (mm^3) in 6-mm diameter	Central subfield thickness (μm)	Average superior thickness (μm)	Average nasal thickness (μm)	Average temporal thickness (μm)	Average inferior thickness (μm)	Average inferior thickness (μm)
Stratus OCT, Carl Zeiss Meditec (Dublin, CA) [24]–[27]	141.02 \pm 12.59, 166.9 \pm 20.9	260.0 \pm 12.2	6.98 \pm 0.37	193.73 \pm 22.23, 198.5 \pm 18.1, 195.6 \pm 17.2, 202 \pm 19.6	244.3 \pm 3, 17.64	261.7 \pm 9, 15.53	226.56 \pm 15.17	232.6 \pm 7, 13.31	232.67 \pm 13.31
Spectralis SD-OCT, Heidelberg Engineering (Heidelberg, Germany) [26], [27]	225.1 \pm 17.1			271.4 \pm 19.6, 271.2 \pm 2.0					
RTVue (Optovue, Inc., Fremont, CA, USA)	175.71 \pm 16.81		7.19 \pm 0.41	208.62 \pm 21.71	252.6 \pm 1, 16.00	257.3 \pm 9, 17.58	238.72 \pm 13.27	239.6 \pm 3, 15.86	239.63 \pm 15.86

[25]								
Cirrus Carl Zeiss (Meditec, Inc., Dublin, CA, USA) [28]	280.33 ± 10.34	10.09 ± 0.37	261.31 ± 17.67	326.2 ± 7 ± 11.89	328.2 ± 7 ± 12.96	313.35 ± 14.20	322.5 ± 3 ± 12.37	339
Topcon (Tokyo, Japan) [24]	263.2 ± 12.6		216.4 ± 18.0					293

OCT optical coherence tomography

Central retinal thickness appears to be related to genetic factors with a heritability estimate of 0.90 [29]. In addition, retinal thickness decreases by 0.26–0.46 μm , macular volume by 0.01 mm^3 , and the retinal nerve fiber layer (RNFL) by 0.09 μm per year. The papillomacular bundle area thins with aging: retinal thinning (due to thinning of RNFL) contributes to 20% and other layers contribute to 80% of this thinning [30].

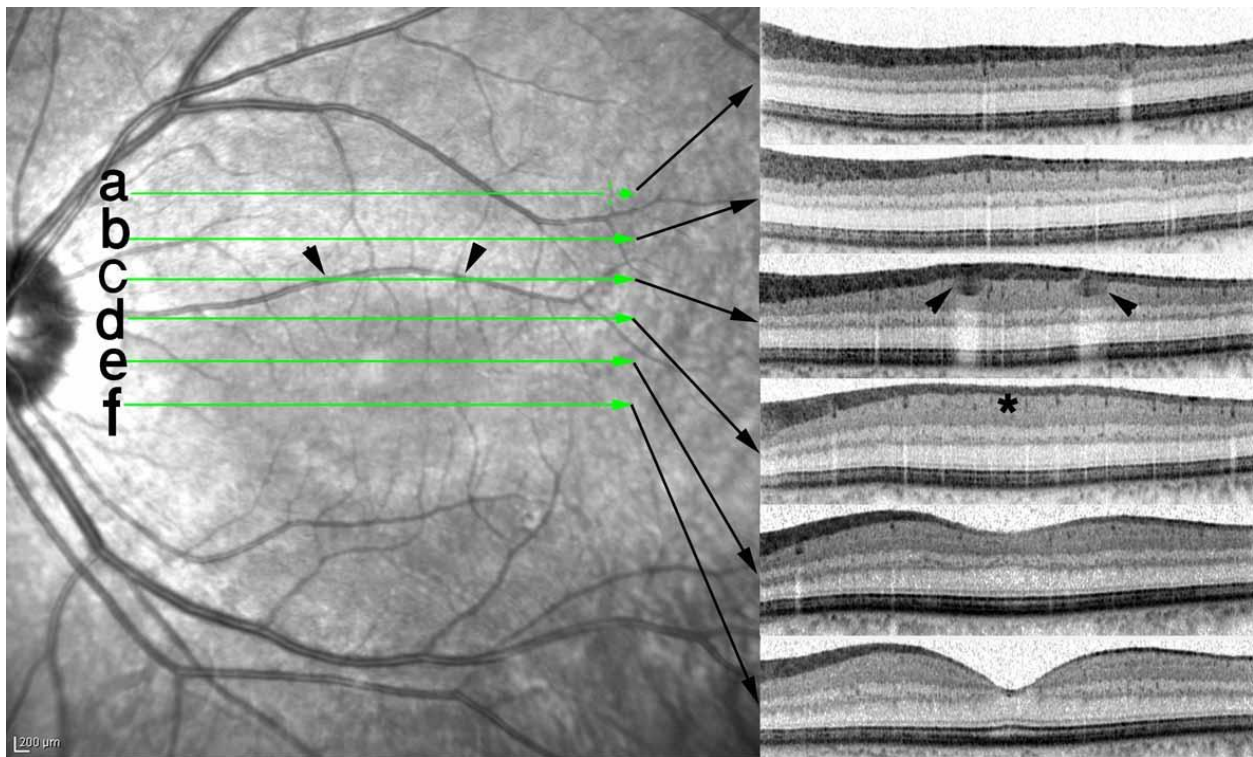


Fig.1. 8 A normal macular optical coherence tomography (OCT) image (left) and scanning laser ophthalmoscopic (SLO) image (right) of the left eye of a patient. The SLO images show the results of six scans (indicated by the letters a–f in the OCT image). The ganglion cell layer is the thickest area in the parafoveal site (*black star*). Shadowing and two hyperreflective points correspond to retinal vessels (*black arrowheads*). The inner layer thickness decreases gradually from the parafoveal site to the peripheral part of the macula. The thickness of nerve fiber layers is

considerably higher on the nasal side than on the temporal foveal side. Thus, the laterality of a horizontal longitudinal OCT image can be estimated without looking at an SLO image

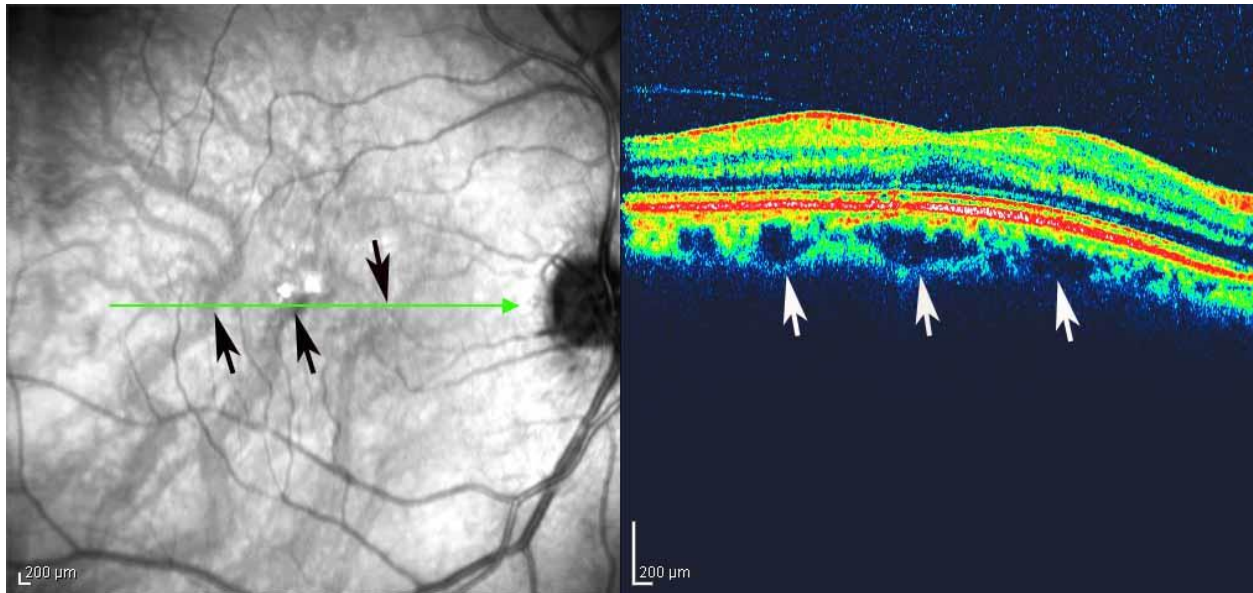


Fig.1. 9 Certain characteristics in a normal optical coherence tomography (OCT) image may be erroneously interpreted as abnormal findings. This image shows engorged and dilated choroidal vessels in an elderly person. The choroid in elderly patients with hypertension often has hyporeflective spaces (*arrows*), which represent dilated engorged choroidal vessels. This feature resembles choroidal varicose veins

III-Anterior Segment Optical Coherence Tomography

Anterior segment optical coherence tomography (ASOCT) is a noninvasive imaging technique that is used to produce high-resolution images from the ocular surface and anterior segment structure. AS-OCT imaging can measure the anterior chamber angle and survey pre-trabecular outflow pathways either qualitatively or quantitatively. Due to rapid development of OCT systems, AS-OCT devices have become into inevitable clinical tools for assessments of the anterior segment and ocular surface.

Mechanism

Izatt et al [31] first introduced ASOCT in 1994 using the same 830nm wavelength of light as retinal TD-OCT. However, anterior segment imaging has different requirements comparing to the conventional posterior segment imaging and

needs a larger width and depth of scan than posterior segment. Here, the anterior segment is more accessible optically than the posterior segment and the light with longer wavelengths can be used in the ASOCT, without concerning about the attenuations normally occur by the vitreous. In addition, by adjusting the numerical aperture, transverse resolution can be increased more than the posterior segment whereas transverse resolution is limited due to a higher level of optical aberrations. As a result, ASOCT often works with longer wavelength sources. Currently, there are two commercially produced dedicated anterior segment devices the SL-OCT and the Visante, which their specification is introduced in Table 1.1. By applying specialized lens adapters, several retinal FD-OCT devices allow imaging of the anterior segment using the shorter wavelength of 830-870nm. Figure 1.10 illustrates ASOCT scan of the normal eye.

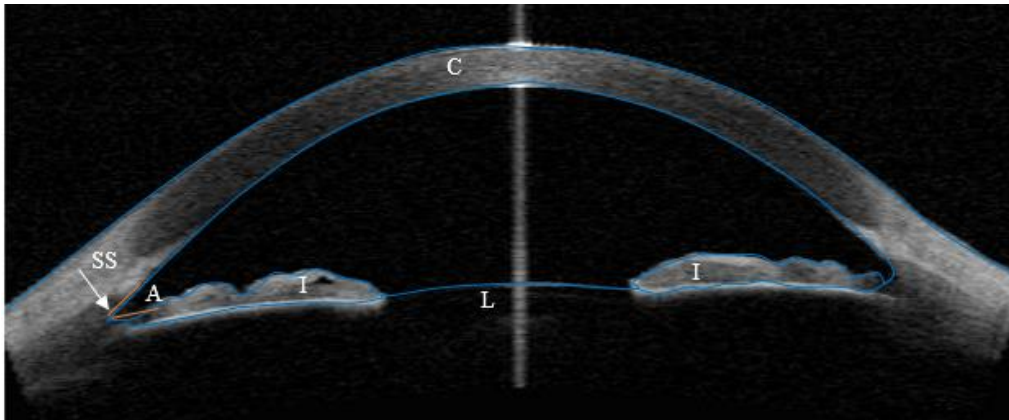


Fig.1. 10 Anterior OCT scan. The cornea (C), iris (I), lens (L), scleral spur (SS, white arrow) and anterior chamber angle (A) are marked for reference.

Clinical applications

AS-OCT can be used in accurate preoperative and postoperative evaluation of blebs, intra-stromal corneal rings, penetrating keratoplasty (PK), descemet-stripping endothelial keratoplasty (DSEK), deep lamellar endothelial keratoplasty (DLEK), IOLs and laser-assisted in situ keratomileusis (LASIK) [32], [33]. AS-OCT can be employed in refractive surgery by anterior chamber biometry. In addition, iris cysts, iris nevus, iris melanoma and iridoschisis can be surveyed by imaging the iris. However, scanning the lens, ciliary body and iris posterior is difficult in this modality due to limitation of light. Glaucoma and corneal disease are two

conventional pathologies which can be assessed and followed by AS-OCT as described in the following (Figure 1.11).

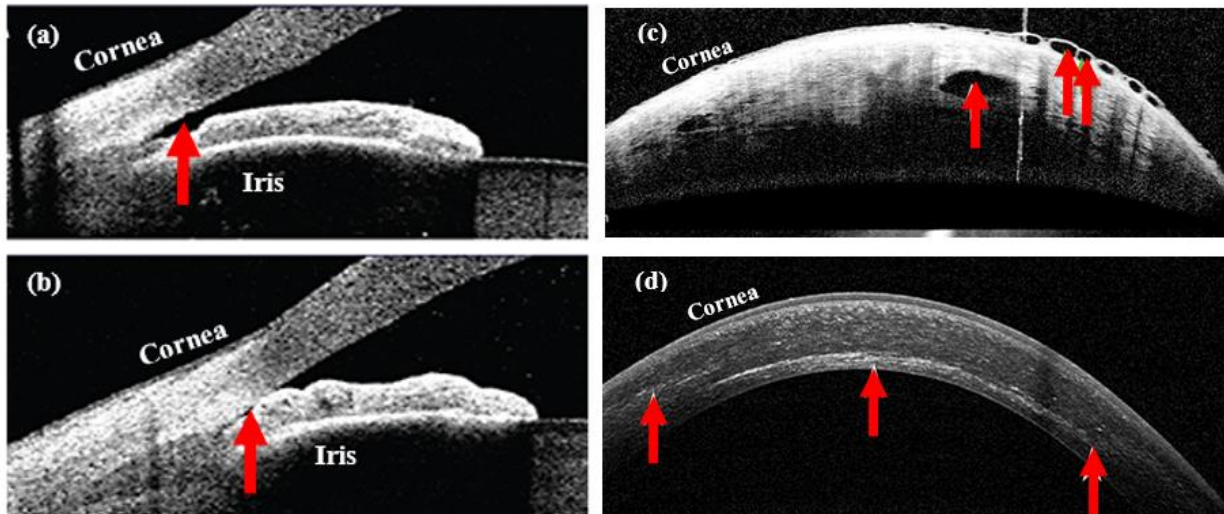


Fig.1. 11 AS-OCT scan of (a) open angle, (b) closure angle (c) severely keratoconic cornea, (d) corneal collagen cross-linking.

Glucoma

Cross-sectional images of AS-OCT helps survey the cornea, angle and anterior chamber. Angle assessment is clinically applied in following, diagnosis and treatment of glaucoma. Angle closure, which is a mechanical blockage of the angle of trabecular meshwork in the anterior chamber, can quantitatively be assessed by AS-OCT to detect primary angle closure glaucoma (PACG) and to identify the scleral spur, Schlemm's canal, Schwalbe's line and trabecular meshwork. Furthermore, AS-OCT can be used in guidance of glaucoma surgeries determining the safety of treatment procedures. In this regard, AS-OCT provides detailed visualizations of the trabeculectomy bleb and several studies have reported an association of bleb morphology with level of IOP control.

Corneal disease

Keratoconus is a bilateral, progressive thinning of the cornea, which is associated with change in collagen structure and decrease in corneal rigidity. AS-OCT has been used to create pachymetry maps to diagnose keratoconus based on asymmetry of the corneal thinning. AS-OCT has been used to measure the efficacy

of collagen cross-linking when treating keratoconus. AS-OCT has also been employed in diagnosis of corneal dystrophies. A summary of selected corneal dystrophies and detailed findings on OCT has been reported by Siebelmann et al. [34]. AS-OCT is an effective complement to biopsy in the diagnosis of ocular surface squamous neoplasia (OSSN). Thickened and hyperreflective epithelial layer and transition from normal to abnormal epithelium are associated with the OSSN.

IV-Enhanced Depth Imaging Optical Coherence Tomography

Enhanced depth imaging optical coherence tomography (EDI-OCT) is a new imaging method that provides very high-resolution visualization of the choroid and the outer part of the globe in detail. It helps in the understanding of the pathophysiology of the choroidal-related conditions.

Enhanced depth imaging optical coherence tomography is easy to perform. By moving the “zero delay line” to the choroid area and averaging a high number of images, a clear image of the choroid and the underlying tissues can be created. This imaging method may change the understanding of pathophysiology and treatment responses in common ocular diseases such as age-related macular degeneration (ARMD), and may change the diagnosis and therapeutic strategies for ocular tumors, uveitis, central serous chorioretinopathy (CSCR), and glaucoma. The choroid is the main vascular bed in the eye and is the primary site affected in many diseases; therefore, its imaging has significant importance. Kim et al. [35] recently claimed that subfoveal choroidal thickness was an indirect indicator of the subfoveal ocular perfusion status.

Mechanism

The choroid lies under the RPE layer and reflects most of the laser light. It is inaccessible using conventional OCT. Increased pixel density and signal-to-noise ratio in spectral-domain OCT (SD-OCT), compared to those of TD-OCT, make choroidal imaging possible. In SD-OCT, structures that are closer to the zero delay line have higher signals than those that are farther away. In conventional OCT, the zero delay line is near the inner surface of the retina; however, in EDI-OCT, the zero delay line is placed near the outer retina and choroid, which is key for EDI imaging. By averaging a high number of images (usually 100 images), the quality of EDI-

OCT increases considerably because of the reduction of “speckles” by the software, which provides high-quality images with a smooth border.

By evaluating OCT images, it is possible to differentiate normal OCT from EDI(Fig 1.12). In normal OCT, the most focused part of the image is the innermost or middle part of the retina. In EDI, the sharpest area is at the RPE level.

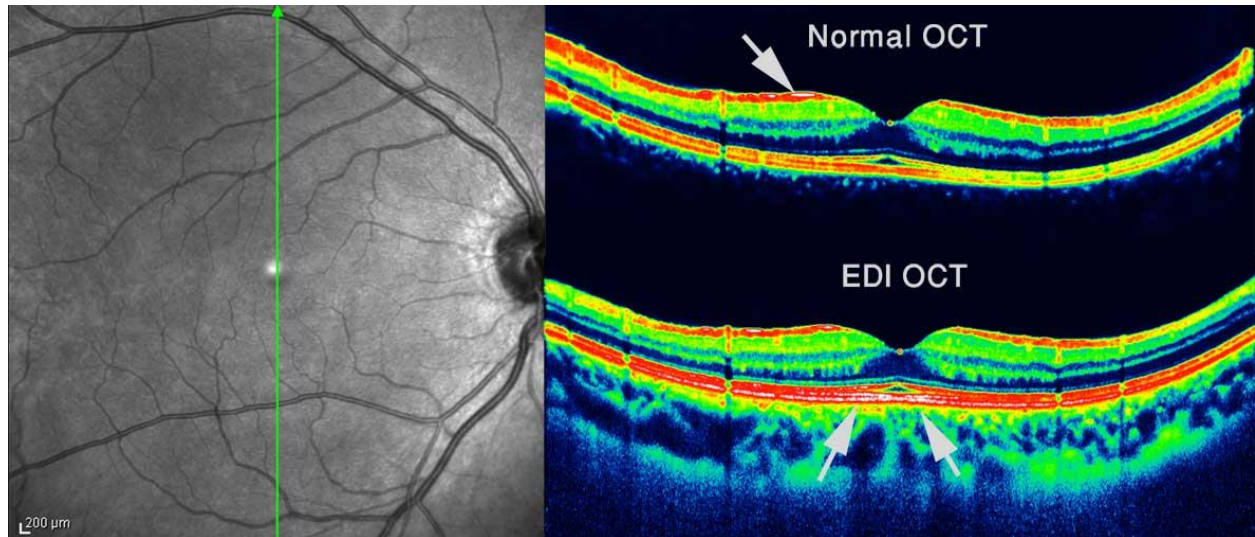


Fig.1. 12 The normal optical coherence tomography (OCT) image and enhanced depth imaging (EDI) OCT image were acquired at the same location in the macula. The white areas in these color images are consistent with points of higher reflectivity and focused areas. In a normal OCT image, the hyperreflective and sharp parts are at the nerve fiber layer level (*white arrow*). In the EDI-OCT image, the hyperreflective white area lies in the retinal pigment epithelium level (*white arrows*)

The quality of an EDI-OCT image may be affected by the following factors: ocular wall distortion such as severe posterior staphyloma that is usually seen in high myopia; a large and elevated lesion at the posterior pole such as a large pigmented epithelial detachment; subretinal fluid collection; accumulation of highly reflective material over the choroid (subretinal, preretinal, or intraretinal) such as hemorrhage, fibrin, and exudates; and a thick choroid or thick lesion that causes the loss of signal penetration and intensity. Other important factors that have a negative impact on OCT image acquisition and are interferers include media opacities and ocular surface disease. In pathologic conditions of the choroid such as polypoidal choroidal vasculopathy (PCV) and central serous chorioretinopathy (CSCR), significant measurement variation should be expected [36], which may be related to the expansibility of the vascular bed of the choroid.

The Heidelberg Company (Heidelberg, Germany) recently introduced a new imaging method, called full depth imaging (FDI)(Fig. 1.13), in which the level of

contrast in the vitreous may be equivalent to that in the choroid. The method is simple: after activating the automatic retinal tracking mode in the normal OCT acquisition method, the EDI mode is activated and the images are acquired when a similar contrast for the choroid and retina appears on the image. In this manner, information from the conventional OCT and the EDI-OCT is available simultaneously in one image. The Heidelberg Company claims that the image quality is similar to that of the swept-source OCT systems (Fig.1. 9).

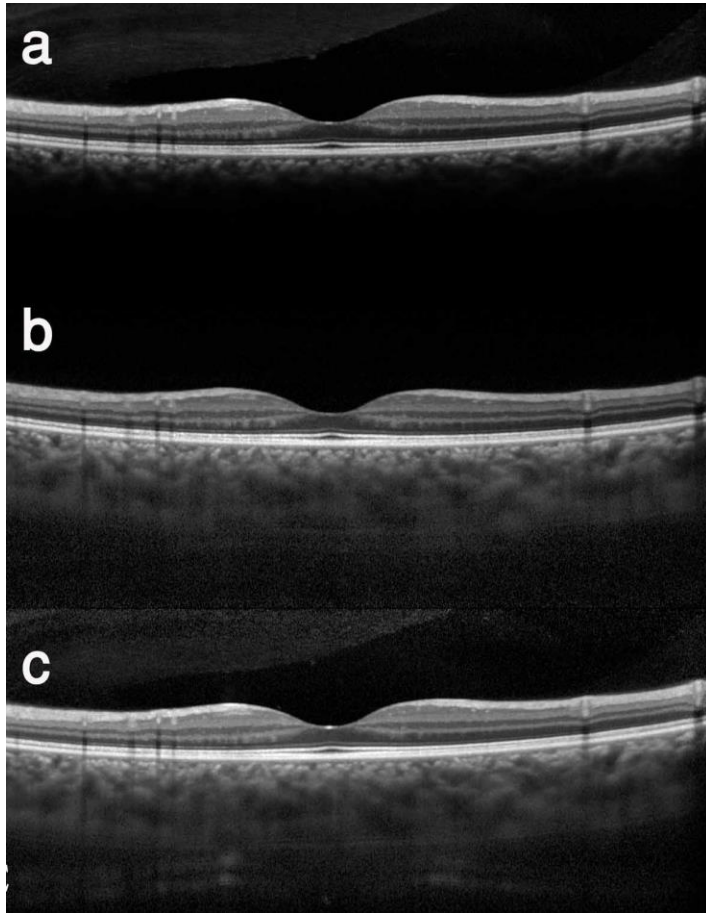


Fig.1. 13 A series of optical coherence tomography (OCT) images of the same point in the retina in **a** the conventional mode (the inner retinal layers reflectance are precise), **b** the enhanced depth imaging (EDI) mode (the inner surface of retina appears slightly imprecise), and **c** the full depth imaging mode (the inner layer and choroid are both clearly defined)

The choroidal anatomy and the vessel map may be clearly defined by EDI-OCT(Fig. 1.14). The choroid is divided in four parts: Bruch's membrane, which is the innermost layer; choriocapillaris; Sattler's layer, which contains medium-diameter blood vessels; and Haller's layer, which is the outermost layer of the choroid (Fig.1. 14).

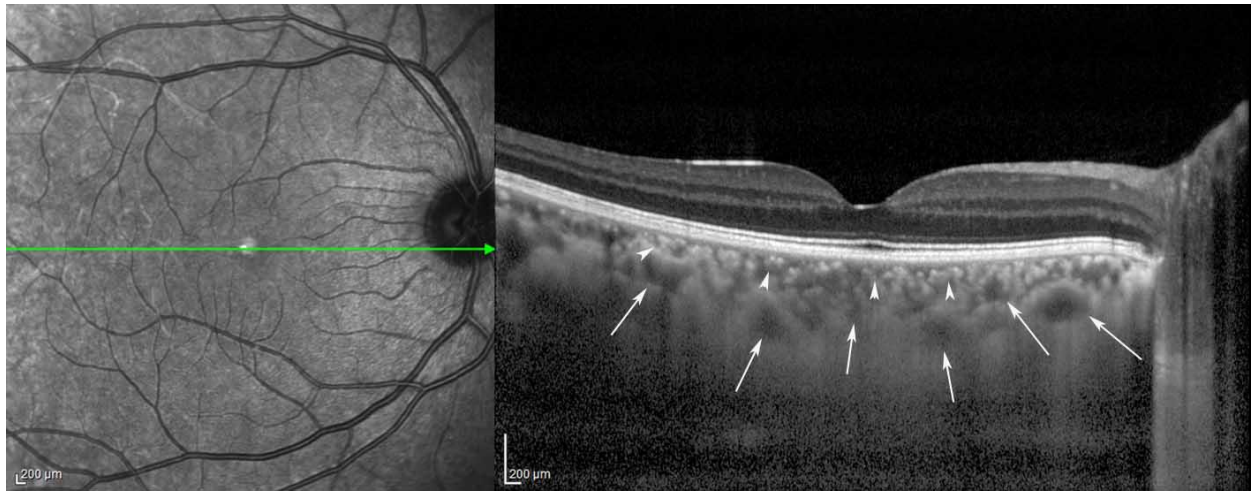


Fig.1. 14 This enhanced depth imaging optical coherence tomography image illustrates the Sattler layer (*white arrow heads*), which contains medium-sized vessels in the choroid, and Haller's layer (i.e., large choroidal vessel layer; *large white arrows*)

In cases of a thin choroid, the sclera and large penetrating vessels may be visible (Fig.1. 15).

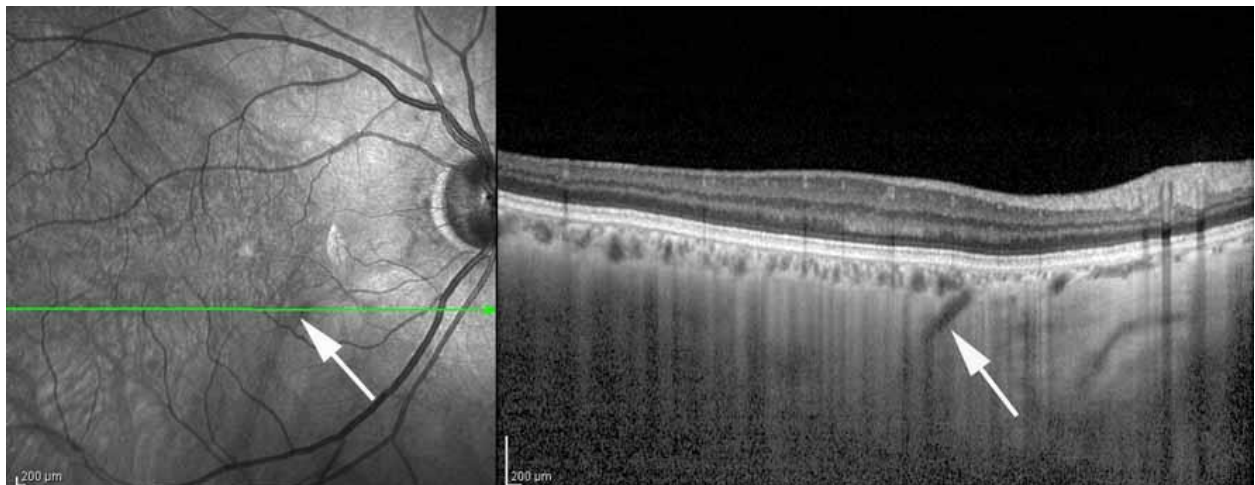


Fig.1. 15 The enhanced depth imaging optical coherence tomography image shows the location and direction of a large, main choroidal vessel penetrating the sclera and the choroidal plexus under the retinal pigment epithelium layer (*white arrow*). The scanning laser ophthalmoscopic image (right) shows this large vessel as a hyporeflective shadow

Aging-related myopia could be associated with thinning of the choroid(Fig.1.16). A young age, tumors, CSCR, hyperopia, and choroiditis are associated with a thicker choroid.

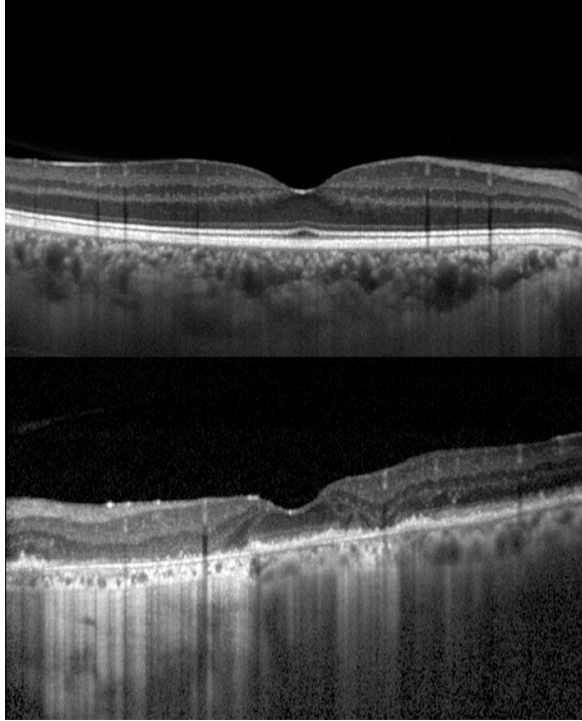


Fig.1. 16 A comparison of choroidal thickness between a 44-year-old person (upper OCT image) and an 85-year-old person (lower OCT image). The difference in thickness is remarkable. With increasing age, the thickness of choroid decreases considerably

When an evaluation of the deeper structures of retina is required—for example, in the case of a large pigmented epithelial detachment(Fig.1.17)—the deeper structures may be evaluated with EDI.

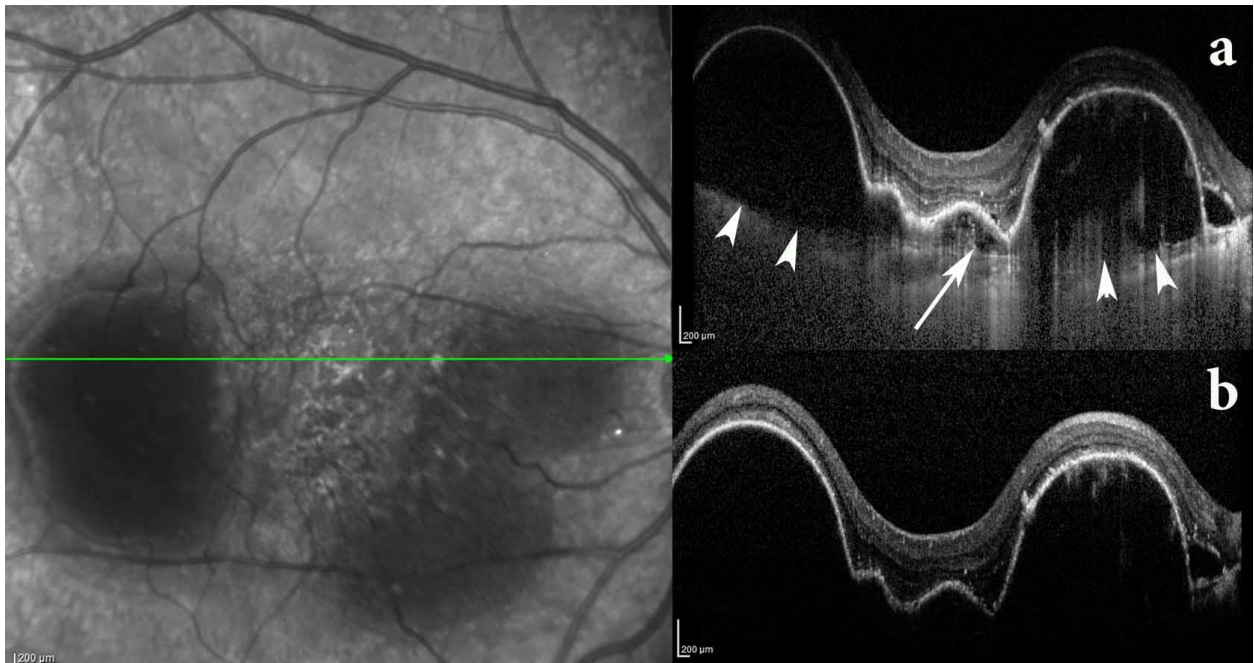


Fig.1.17 A patient with large and multilobulated pigmented epithelial detachments (PEDs). **a** The enhanced depth imaging optical coherence tomography (EDI-OCT) image. **b** The conventional scanning laser ophthalmoscopic optical coherence tomography image. Bruch's membrane boundaries (*white arrowheads*) are visible in the EDI-OCT image. Vascular networks in the neovascular PED at the center of macula (*white arrow*) are visible with EDI-OCT and cannot be demonstrated with the conventional method

Clinical Applications

Choroidal Measurements

The most important application of the EDI is the evaluation of choroidal thickness, volume, and thickness map, which may be altered in diseases such as ARMD, CSCR, uveitis, and choroidal tumors. The retinal thickness measurement is more precise, compared to choroidal thickness measurement. This factor is partly related to the higher variation in choroidal thickness, compared to that of the retina [37]. However, defining the chorioscleral interface accurately is sometimes inconsistent because the definition of the outer boundary of choroid may be imprecise. An imprecise definition of the outer boundary may also explain the wide variation of choroidal thickness among recent reports.

In 2009, Margolis et al. [37] and in 2010, Manjunath et al. [38] evaluated choroidal thickness by using the Spectralis OCT apparatus (Heidelberg Engineering, Heidelberg, Germany) and the Cirrus HD-OCT apparatus (Carl Zeiss Meditec, Inc.). Subfoveal choroidal thickness was estimated as $287 \pm 76 \mu\text{m}$ by Spectralis OCT and $272 \pm 81 \mu\text{m}$ by Cirrus HD-OCT. The researchers determined that the thickest choroidal part was in the inferior foveal region.

An OCT apparatus that provides a longer source light wavelength, called high-penetration OCT (HP-OCT), allows higher penetration through the RPE, and thereby enables deep choroidal imaging. Recent studies have also concentrated on thickness map measurements using HP-OCT. However, Ikuno et al. [36] reported that a comparison of EDI-OCT and HP-OCT were highly consistent in the measurement of the choroid. The choroidal thickness (Fig. 1.18) was measured as $292.7 \pm 77.3 \mu\text{m}$ using HP-OCT and as $283.7 \pm 84.1 \mu\text{m}$ using Spectralis (SD-OCT system).

One study [37] also showed that choroidal thickness and choroidal thickness mapping had high reliability and reproducibility. Agawa et al. [39], Hirata et al. [40], and Esmaeelpour et al. [41] measured the mean choroidal thickness with swept-source OCT. The results varied widely: the choroidal thickness ranged from $191.5 \pm 74.2 \mu\text{m}$ in the Hirata study to $341 \pm 95 \mu\text{m}$ in the Esmaeelpour study. The thinnest part of the choroid in all of these studies seemed to be the nasal macula (Fig. 1.18).

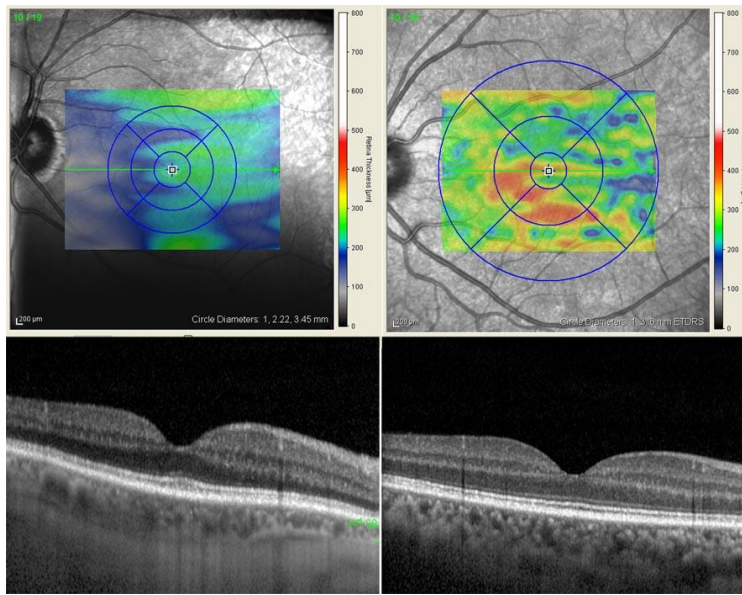


Fig. 1.18 These two choroidal topographic maps have been manually obtained from two male patients of different ages. The left images show the choroid of a 75-year-old man and the right images show the choroid of a 36-year-old man. This compound figure demonstrates the impact of age on choroidal thickness

Choroidal Tumors

The other and perhaps the most important application of the EDI-OCT is related to the diagnosis and monitoring the treatment of choroidal tumors. This information could not be obtained by other modalities with the same level of detail as that obtained by the EDI-OCT. This is widely elaborated in the ocular tumor section of this book.

Another main application of EDI is for differentiating choroidal tumors from ocular wall distortion such as posterior staphyloma and choroidal atrophy secondary to trauma or inflammation (Fig.1.19). Therefore, to rule out choroidal mass or tumor, the use of EDI-OCT is recommended for every patient for whom the conventional OCT image indicates ocular wall distortion. Furthermore, the outer boundary of choroidal layer should be verified in such cases to avoid missing choroidal tumors.

Age-related Macular Degeneration

A variable amount of choroidal thickness has been reported among patients with wet-type ARMD or dry-type ARMD [42], although the choroid becomes thinner with age [43]. This finding may be related to the type of age-related changes; it has been shown that subfoveal choroidal thickness is less in eyes with only reticular

pseudodrusen, compared to eyes with early ARMD and eyes having five or more medium drusen (63–124 μm) or any large drusen ($>125 \mu\text{m}$) within the macula without pseudodrusen [44].

Subfoveal choroidal thickness in patients with PCV (285.9 μm) is greater than that in normal individuals, and subfoveal choroidal thickness is considerably lower in patients with wet-type ARMD (119.4 μm) than in normal individuals (186.77 μm) [45]. This finding suggests that EDI-OCT is an auxiliary test for differentiating ARMD from PCV [46].

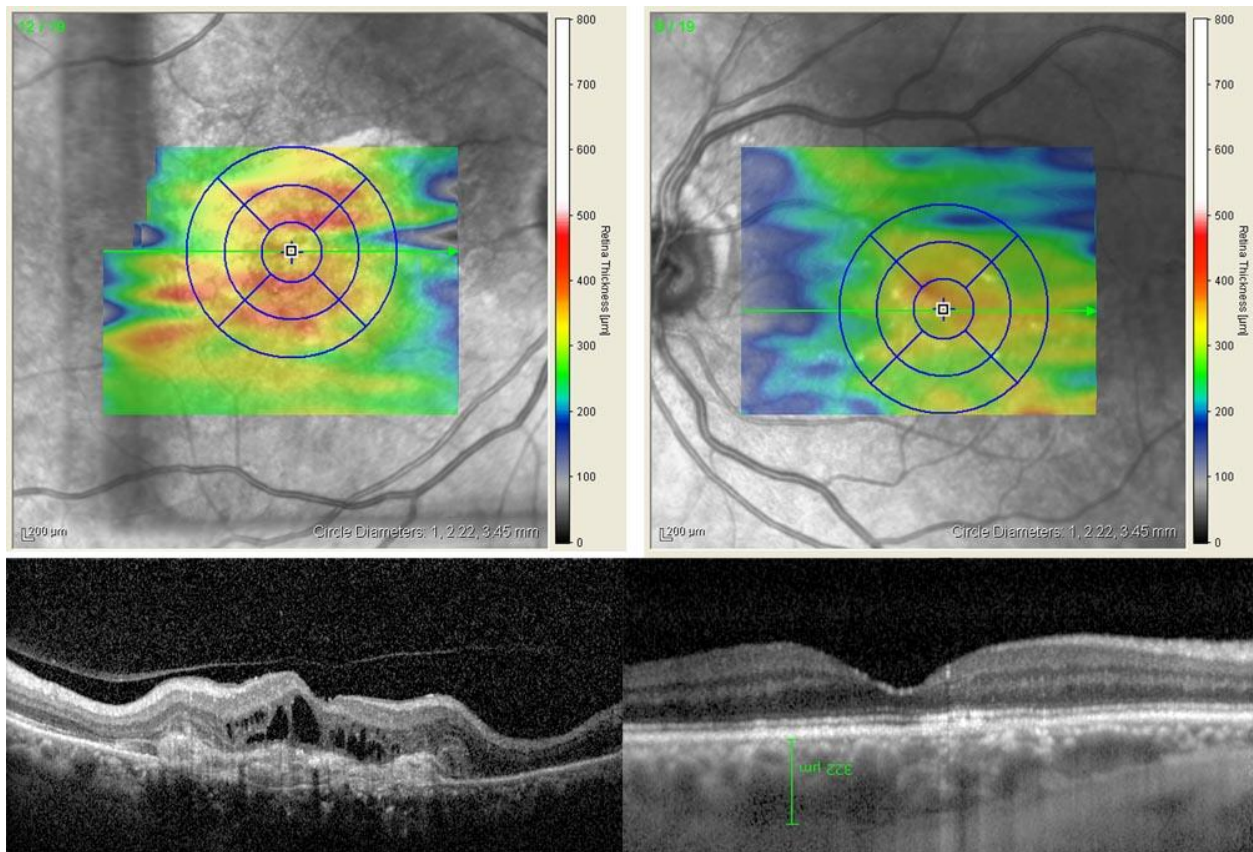


Fig.1. 19 The compound image shows the choroidal topographic map of both eyes of a patient with wet-type age-related macular degeneration (ARMD) in the right eye and early type ARMD in the left eye. The choroidal volume in the right eye is higher at the central foveal area, compared to the left dry eye

Diabetic Retinopathy

Diabetes is a vascular disease; thus, significant changes can be expected in the choroid of diabetic patients. Kim et al. [47] reported that choroidal thickness increased with the increasing severity of diabetic retinopathy from mild/moderate nonproliferative diabetic retinopathy to proliferative diabetic retinopathy. Ki, also

found that choroidal thickness was significantly reduced in patients with panretinal photocoagulation, and the choroid was thicker in patients with diabetic macular edema, especially in those who had subretinal detachment. Therefore, using EDI-OCT for diabetic patients allows the verification of the status of diabetic retinopathy.

In addition, some investigators claim that in diabetes type two, the overall choroidal thickness decreases [48], and this disease may trigger ischemia and eventual pathological events in diabetic eyes such as diabetic macular edema.

Central Serous Chorioretinopathy

Central serous chorioretinopathy (CSCR) is a disease characterized by the detachment of the neurosensory retina, diffused hyperpermeability of the choroidal vessels on ICG angiography, and active RPE leakage on fluorescein angiography, all of which suggest generalized choroidal vascular disturbance [49]. Increased choroidal thickness is the hallmark of CSCR, and has been demonstrated in previous studies [50]–[52](Figure 1.20).

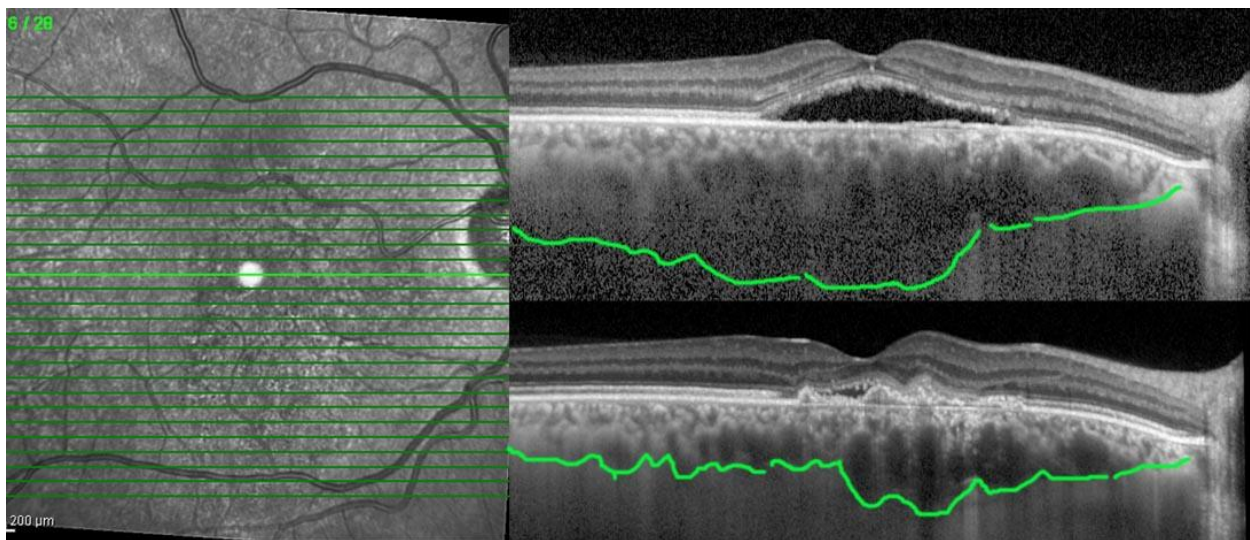


Fig. 1.20 The compound image shows chronic active central serous chorioretinopathy in a patient who was treated with photodynamic therapy (PDT). The upper longitudinal enhanced depth imaging optical coherence tomography shows subfoveal serous detachment with considerable choroidal thickening (*traced with a green line*). After PDT, serous fluid resorbed completely with some residual retinal pigment epithelium changes. Choroidal thickness, which is delineated by the green line, shows considerable thinning

Recent EDI-OCT studies have revealed a thinned inner choroidal layer and enlarged underlying hyporeflective choroidal lumina. Dome-shaped RPE elevation,

a double-layer sign of the RPE/Bruch's membrane complex, and RPE microrips are other findings on EDI-OCT of patients with CSCR [53].

Glaucoma

Using EDI-OCT, some authors have claimed that the lamina cribrosa at its central and midperipheral parts is situated more posteriorly in glaucomatous eyes [54]. The focal loss of laminar beam or even acquired pit in cases of advanced glaucoma has been observed by some groups [35], [55]. In addition, a deep optic nerve complex in glaucomatous eyes is another finding that Park and his colleagues [56] discovered by using EDI-OCT. In the future, EDI imaging of the optic nerve may be a diagnostic imaging modality for patients with glaucoma. Age-related choroidal atrophy puts patients at a higher risk for glaucoma [43].

Uveitis

The choroid is the origin of most posterior uveitis and intraocular inflammation. A well-known intraocular inflammation is Vogt–Koyanagi–Harada (VKH) disease. It requires long-standing treatment with corticosteroids. However, the time that the drug should be tapered and discontinued is an area of debate. The evaluation of choroidal structure and thickness is helpful in assessing treatment efficacy or recurrence of the disease.

A thickened choroid is the hallmark of VKH disease. This is related partly to inflammatory infiltration and partly to exudation. After steroid treatment, the choroid quickly becomes thinner. Therefore, EDI-OCT may prove useful for managing and for diagnosing VKH disease [57]. (Fig.1.21)

Choroidal thickness may also serve as a marker for the degree of inflammation in VKH disease [58]. Some EDI-OCT studies on VKH disease reveal that, compared to control patients, patients with VKH disease have a significant loss of focal hyperreflectivity in the inner choroid in the acute and convalescent stages of the disease (Figure 1.21). In the acute phase, the choroid is thicker than in the convalescent phase [59]. However, in long-standing disease, progressive choroidal thinning is evident [60].

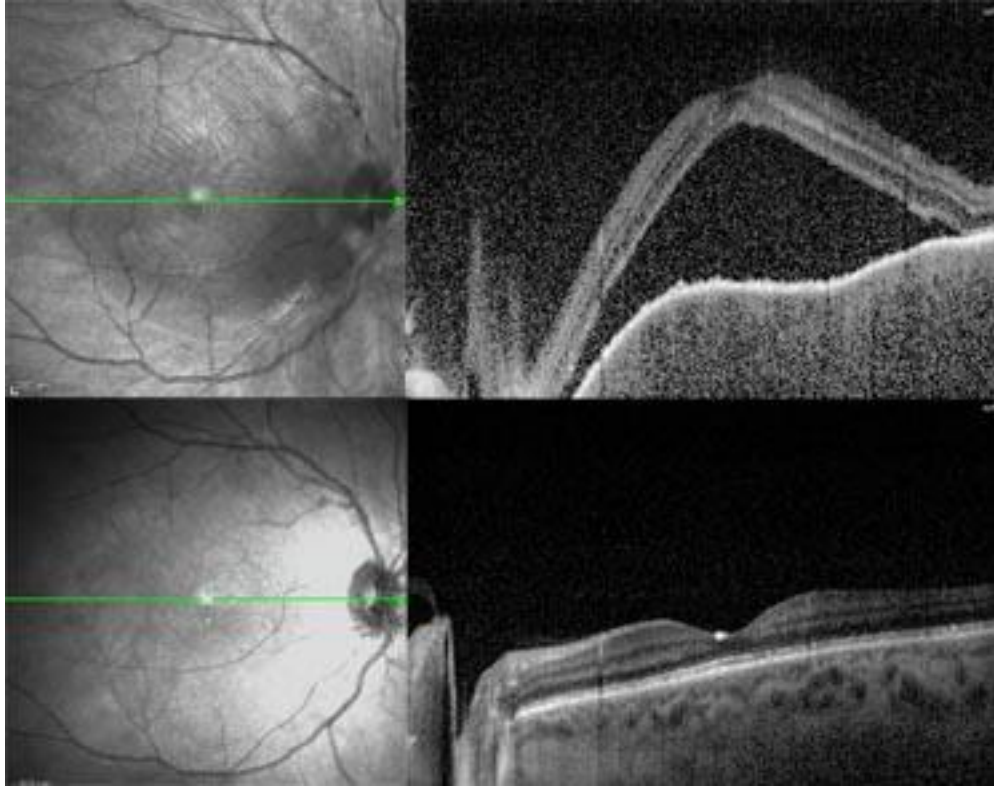


Fig.1. 21 These two enhanced depth imaging optical coherence tomography (EDI-OCT) images were taken in the acute phase (*upper panels*) and after treatment (*lower panels*) in a patient with Vogt–Koyanagi–Harada (VKH) disease. Choroidal homogeneity and the disappearance of the choroidal vasculature is an EDI-OCT finding in patients in the acute phase of the VKH disease; the choroid returns to the normal condition with treatment

In fact, few reports exist on the use of EDI-OCT in patients with other types of intraocular inflammation. Yasuno et al. [61] evaluated a patient with multifocal choroiditis, and found localized thinning of the choroid, occlusion of the choroidal vessels, and localized hyperreflectivity that may have represented hyperpigmentation of the choroid.

Myopia

Owing to the thinner choroid in myopic eyes, EDI-OCT may detect deeper structures such as the sclera and large vascular networks. For each decade of life, subfoveal choroidal thickness decreases by 11.9–12.7 μm , and for each diopter of myopia, by 6.21–8.7 μm [44], [62]. The mean subfoveal choroidal thickness varies from $93.2 \pm 62.5 \mu\text{m}$ to $213 \pm 58 \mu\text{m}$ in multiple studies [41]. some researchers [61] also postulate that choroidal thickness is inversely correlated with age, refractive error, and visual acuity.

By using EDI-OCT, it is possible to measure scleral thickness in myopic eyes [63]. In highly myopic eyes, the dome-shaped macula is the convex elevation of the macula. Enhanced depth imaging optical coherence tomography reveals that this feature results from relative localized thickness variations in the sclera under the macula [64].

V- Optical Coherence Tomography Angiography

Ocular diseases cause vascular abnormalities that is usually captured using approaches such as fluorescein angiography (FA), and indocyanine green angiography (ICGA), which are invasive dye-based techniques. However, intravenous injection of a contrast agent (dye) can lead serious side effects in both FA and ICGA. OCTA is a novel, noninvasive imaging technique that produces angiographic images without using dye [65]. It can produce high-resolution 3D retinal and vascular angiograms and capture the position of vessels by the variations of OCT signal caused by flowing red blood cells. Comparing to dye-based techniques, this modality can facilitate the diagnosis important eye diseases in a faster, more confident, and more repeatable manner. OCTA works based on the detection of the motion of blood cells and uses intrinsic signals to localize the blood vessels. It has been shown that this imaging modality may be useful for the evaluation of common ophthalmologic diseases such AMD, diabetic retinopathy, artery and vein occlusions, and glaucoma.

The first commercial OCTA system was launched in 2014 [66], and rapidly became a ubiquitous standard OCT technology. Despite the insensitivity of OCTA to the leakage, relatively small field of view, and increased potential for artifacts, it can potentially improve the knowledge of eye physiology and pathophysiology.

Mechanism

Since the blood flow varies the OCT signals more than static tissue, OCTA signal increases relevant to the speed of the flowing up to a saturation limit. Multiple approaches such as signal intensity changes, phase changes or both of them can follow these variations. Hence, by acquiring many B-scans from the same position and comparing them a map from blood flow is produced. Sequential imaging from

the same location requires a very high imaging speed to provide approximately 6 seconds for the construction of each three-dimensional (3D) scan set. That is why the development of OCTA occurred after introduction of Fourier-domain OCT systems which increased the scanning speed of OCT by a factor of 50. OCTA can provide a 3D dataset representation of vascular portion of the target tissue.

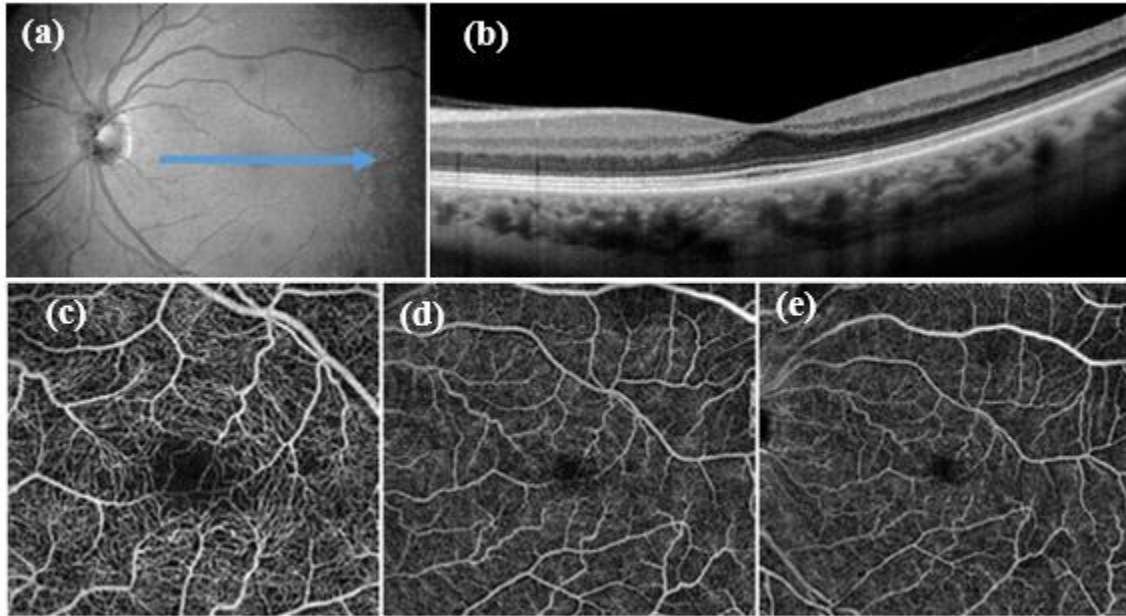


Fig.1. 22 Fields of view and segmentation layers of OCTA. (a) En-face intensity OCT image, (b) OCT b-scan image, (c) Full-thickness 3×3 mm OCTA, (d) Full-thickness 6×6 mm OCTA, (e) Full-thickness 8×8 mm OCTA.

The viewer can scroll among the projection images (i.e., OCT angiograms) from the internal limiting membrane (ILM) to the choroid and view retinal structures. Moreover, the layers, slabs, between two relevant boundaries of the specified tissue can be represented through 2D enface images as well. Figure 1.22 is an OCTA image of the normal macular structure.

The cross-sectional method is another representation of the angiograms. In this method, colors are specified to the flow signal overlaying it on the structural OCT image. In this way, the depth of vascular abnormalities such as choroidal neovascularization (CNV) can be screened in details (refer to Figure 1.22). Nowadays, four OCTA devices are commercially used for cilinical applications, which are compared in Table 1.3. These devices have different software for visualization of volumetric data, and segmentation which causes significant

variability in clinical performance such as image quality, vessel visibility, and motion artifacts [67].

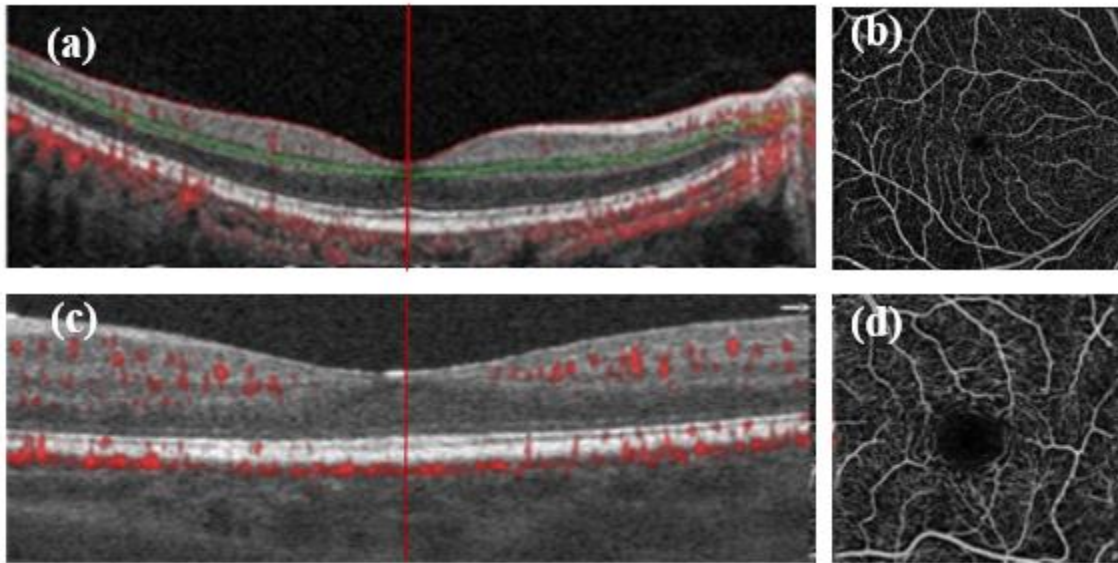


Fig.1. 23 (a), (c) Cross sectional OCT with angio flow (denoted in red) and the corresponding enface OCTA (b), (d) of the superficial capillary plexus.

Table 1.3: Summary of the commercially available OCTA devices

Company	OCTA system	Algorithm	Optical source, nm	Scan speed	Resolution (Axial × Transverse, Microns)	Imaging Depth, mm	Imaging Size, mm	Imaging Volume	Theoretical Acquisition Time, s
Zeiss	AngioPlex	OMAGC	840	68,000	5 × 15	2	3 × 3, 6 × 6	245 × 245, 350 × 350	3.6
Optovue	AngioVue	SSADA	840	70,000	5 × 15	2.0-3.0	3 × 3, 6 × 6, 8 × 8	304 × 304, 400 × 400	3
Topcon	SS-OCT-Angio	OCTAR A	1050	100,000	8 × 20	2.6	3 × 3, 6 × 6	256 × 256, 320 × 320	2.7

Heidelberg	Spectralis OCTA	Amplitude De-correlation	870	85,000	5 × 6	2	3 × 3	256 × 256, 512 × 512	5.4
Nidek	AngioScan	Modified OMAG	880	53,000	7 × 20	2.1	3×3 to 9× 9	256 × 256	2.5
Canon	AngioeXpert	No data	855	70,000	No data	No data	3×3 to 8× 8	No data	3

Clinical application and limitations of OCTA

OCTA provides a depth-resolved retinal vasculature visualization similar to histologic studies. This imaging modality is dye-free and removes the problems of dye-associating techniques. It also provides better visualization of the deep capillary plexus and choroid than FA and ICGA [68]. However, OCTA requires multiple scanning of the single location, which is time consuming for scanning larger areas. In addition, hardware and software of OCTA devices are different in various manufacturers. Each device has a dedicated programming algorithm for flow detection and image size, which can affect imaging results in terms of vascular details. That is, to accurate follow-up a special disease, patient images should be acquired on the same device. Moreover, dye leakage, which is a common landmark in inflammatory vascular pathology, cannot be visualized by OCTA. It cannot measure the vascular filling too. Aside developments in providing larger scan patterns, OCTA has still limited ability to capture retinal periphery and detect pathology there.

Generally, if the clinicians achieve appropriate training to interpret OCTA data and find proper landmarks, OCTA has a promising future. OCTA has been already used as a powerful tool for capturing the retinal vascular disease, retinal inflammatory disease, retinal tumors and retinal hereditary dystrophies which will be described in the following.

OCTA of Diabetic Retinopathy

Studies show that OCTA can determine vascular changes in diabetic patients [69]. It can be reliably used to identify early changes in diabetic eyes, and follow the disease in patients with Diabetic retinopathy (DR) due to accurate assessing foveal avascular zone (FAZ) enlargement over time. By using OCTA, FAZ area can be assessed on the full retinal depth projection. This eliminates the segmentation step and accompanying errors and increases measurement's reproducibility [70]. (Refer to Figure 1.24)

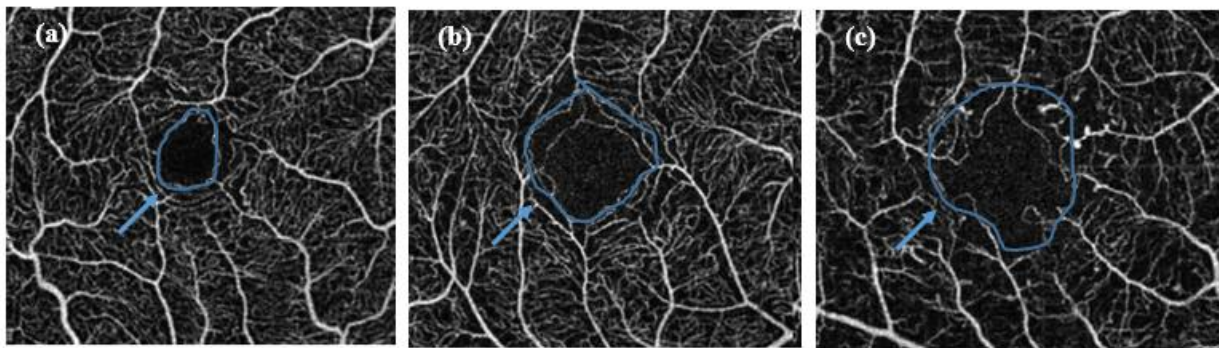


Fig.1. 24 OCTA scans of the three different groups of nonproliferative diabetic retinopathy (NPDR). (a) mild, (b) moderate, (c) severe.

In addition, by visualizing approximately 60% of the Microaneurysms (MA) identified on foveal avascular (FA), OCTA can be incorporated in landmark finding in DR, which are associated with the high risk of progression to advanced diabetic stages [71]. Moreover, it has been shown that there is associations between vascular changes captured by OCTA and increasing the severity of DR [72]. Color-coded perfusion maps of OCTA can capture the vessel density and help clinicians track DR severity and survey the vessel loss in association with disease progression. (Refer to Figure 1.25)

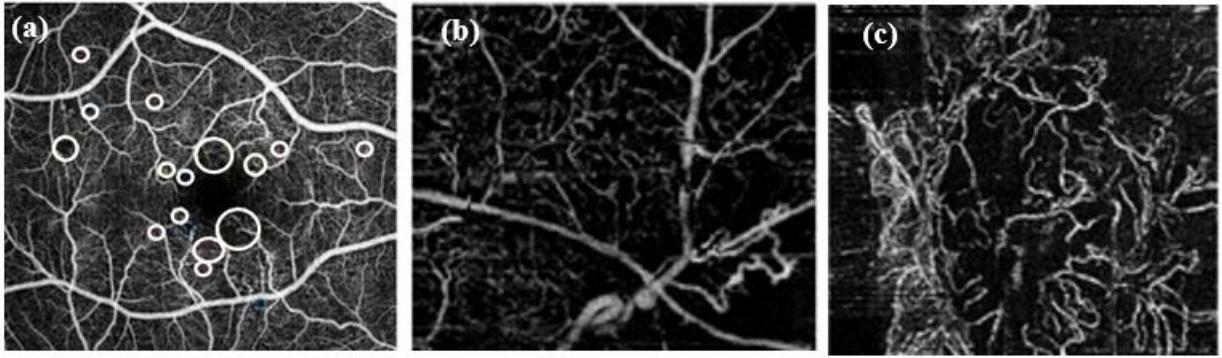


Fig.1. 25 OCTA scans of the three different groups of nonproliferative diabetic retinopathy (NPDR). (a) OCTA with FAZ enlargement, MA are circled white. (b) OCTA with abnormal vessels in an area of capillary non-perfusion. (c) OCTA with the NVD, which is clearly appreciable.

OCTA of Non-Neovascular AMD

OCTA can visualize the choriocapillaris in intermediate AMD and later stages of the disease due to the decreasing of choriocapillaris flow in dry AMD, which can be identified by choroidal vasculature changes, and blood flow captured by the OCTA [73] (refer to Figure 1.26). Moreover, several publications investigated the ability of OCTA for detection of the neovascular complexes associated with wet AMD by analysis of choroidal neovascular membranes (CNVM) [74].

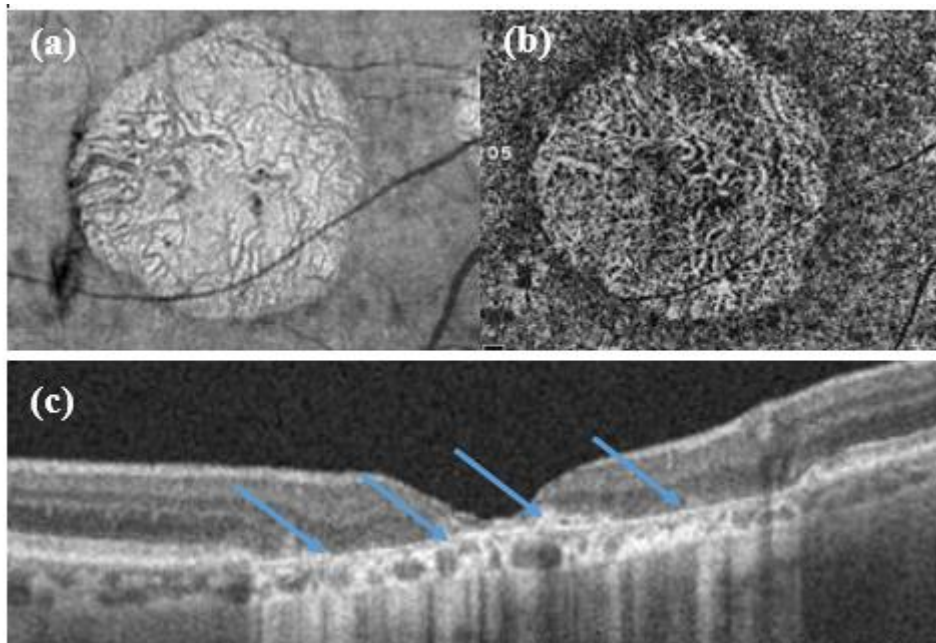


Fig.1. 26 Geographic atrophy (GA) associated with dry AMD which can be easily observed on (a) en face OCT (b) OCTA scan at the level of the choriocapillaris, and (c) structural OCT.

OCTA of Glucoma

OCTA is also going to be popular for assessment of optic nerve disorders, such as glaucoma. This modality can capture the attenuated peripapillary and macular vessel density associated with pre-perimetric glaucoma (Figure 1.27). Therefore, it can hopefully be incorporated in the early detection of glaucomatous damage. Moreover, it can be used in analysing metabolic activity of the retinal inner layers and thus provide progression monitoring in this disease [75].

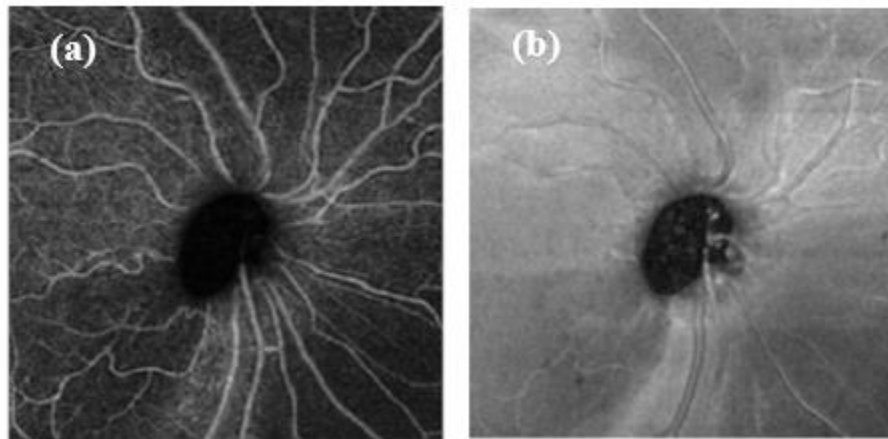


Fig.1. 27 - OCT-A (a) and *en face* structural imaging (b) of a glaucoma patient. It can be seen that Inferior temporal of retinal fiber layer is lost and the vessel density is decreased.

VI-Limitations and Indications of OCT

A limitation of OCT primarily originates from the limitation in its penetration depth (1500 microns). However, it is not possible to scan certain distant peripheral areas (i.e., farther than the midperiphery, $>60^\circ$). The signal-to-noise ratio, which represents the quality of an image, is also another factor that influences clinicians' ability to use this imaging modality. For media opacity, the use of OCT is limited because of poor penetration of the laser rays. Despite the latest techniques and decreased acquisition time, patient cooperation and positioning remain vital for obtaining a high-quality image. However, OCT cannot be used to evaluate

functional problems. Therefore, additional tests such as angiography are sometimes needed for assessing retinal and ocular function.

Optical coherence tomography is an essential part of ocular and retinal examination in most patients who are referred for retinal etiology-related visual loss. Therefore, OCT would be a convenient and first-choice imaging modality for the evaluation of macular status, fine thickness measurement and changes (by serial OCT), following treatment plans and planning for surgery, diabetic macular status, retinal vascular accident, age related macular degeneration, high myopia, central serous retinopathy and choroidal evaluation OCT would be easy and first choice imaging modality.

VII-Pitfalls and Artifacts

Artifacts

Optical coherence tomography has multiple artifacts. In 2005, Ray et al. [76] first described artifacts in TD-OCT. These artifacts also can occur with an SD-OCT apparatus. Ray described six types of image artifacts in TD-OCT that can be classified into two groups:

(1) misidentification of the inner or outer retinal layer (Fig.1.28) and (2) out-of-register artifact (Fig.1.29), artifacts caused by degraded image, cut edge artifact, and off-center artifacts. The first group of artifacts is caused by the computer software misidentifying retinal surfaces or by retinal pathologies that result in retinal layer disorganization and disruption that create software identification mistakes. The second group is caused by poor image acquisition or quality.

Some other artifacts that exclusively occur with an SD-OCT apparatus are based on Fourier domain detection that cannot differentiate negative from positive time delay such as mirror artifacts [77]. This artifact produces symmetrical OCT images around the 0-delay line. It can primarily occur in highly myopic eyes and in lesions with a high axial diameter such as elevated ocular tumors or detached retina. Misidentification of the inner or outer retinal layer or artifacts that are caused by degraded image are examples of segmentation errors. It occurs overall in 77% of OCT scans with different OCT apparatuses [78].

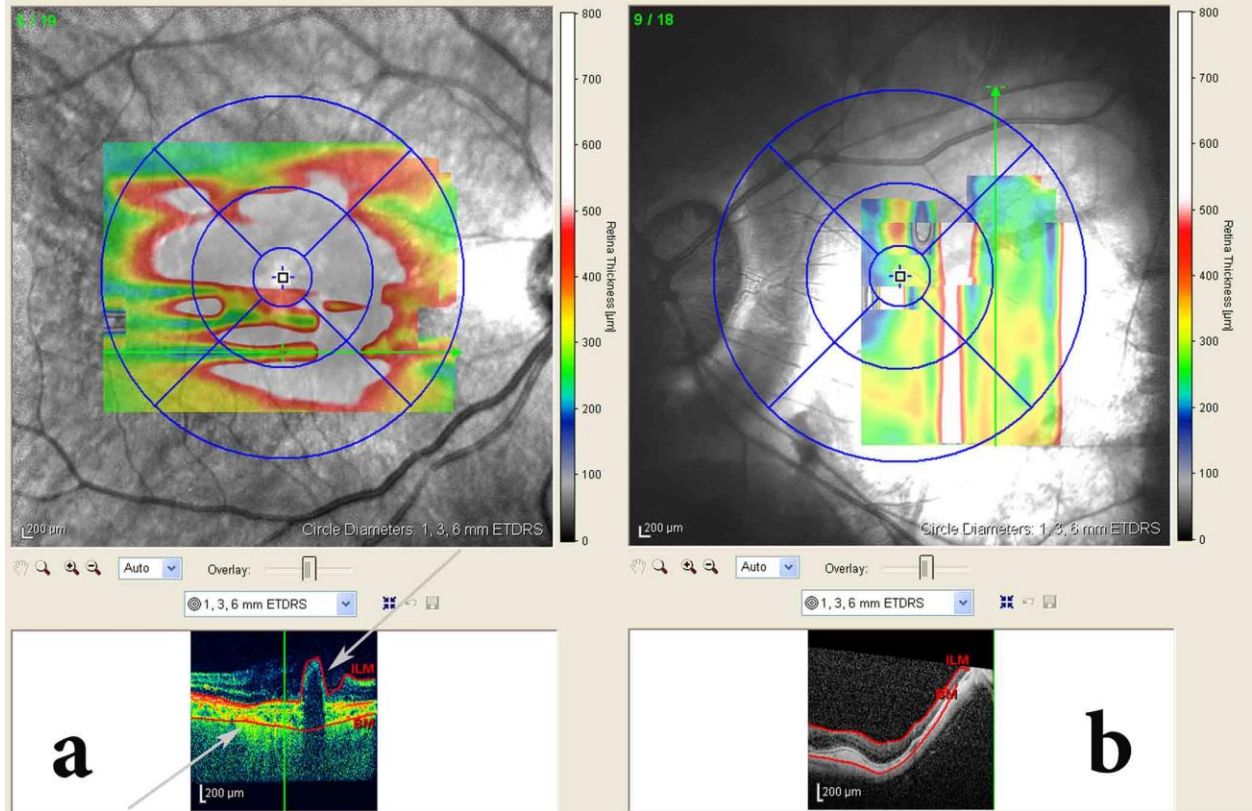


Fig.1. 28 a Misidentification of the retinal layer in a patient with late age-related macular degeneration (ARMD) results in an unreliable topographic map (*grey arrows*). **b** The topographic map of a patient with posterior staphyloma is affected by a misidentification error. The optical coherence tomography apparatus recognizes the outer scleral border as the retinal pigment epithelium layer, which results in corruption of the topographic map

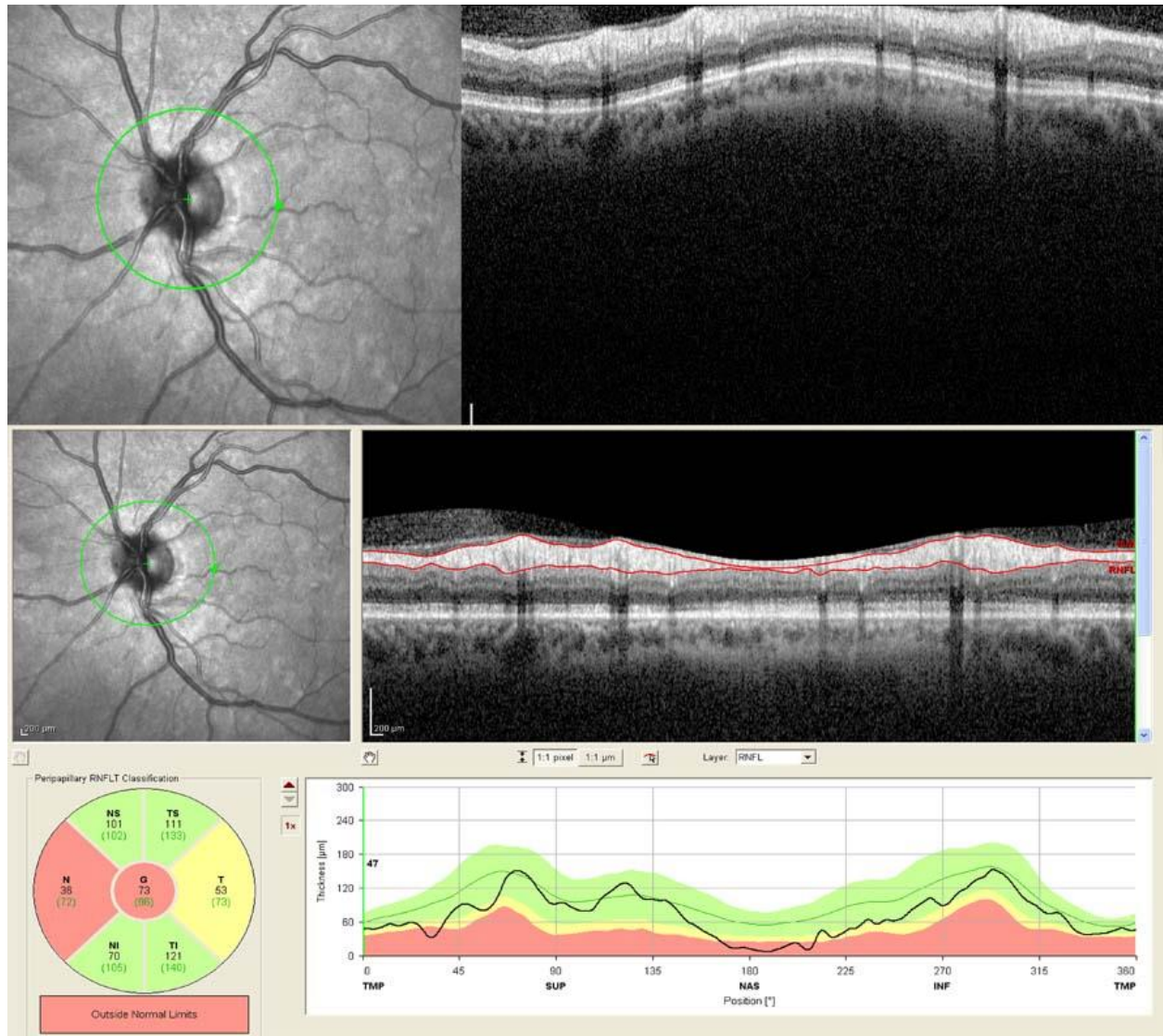


Fig.1. 29 An example of an out-of-register artifact. The image acquisition is incorrect and the out-of-register field subsequently has an abnormal nerve fiber layer thickness profile

The OCT scan is the best method for evaluating the retinal structure. However when analysis protocols are applied, a hyperreflective lesion can cause software-related artifacts. To prevent this error, a review and reevaluation of the clinical retinal examination should be performed for anyone in whom the OCT findings are inconsistent with the clinical findings [79].

Shadowing is among the most common artifact in OCT. Shadowing is caused by the presence of an obstacle in front of the retinal layer (e.g., vitreous opacities, blood, calcification, membranes), which prohibits the passage of laser waves and reflectance waves(Fig.1.30). Sometimes shadowing causes considerable blurring on an image or a misdiagnosis.

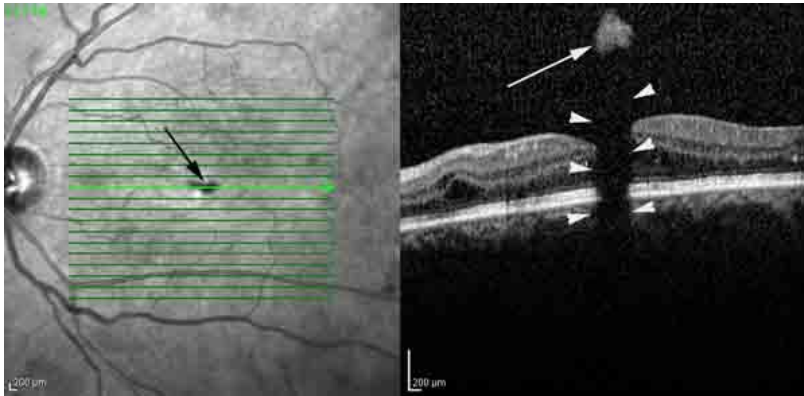


Fig.1. 30 Scanning laser ophthalmoscopy optical coherence tomography images exhibit the artifact of shadowing because a small dense vitreous opacity (*black arrow*) interfered with laser wave penetration. The direction (*white arrowheads*) of the shadowing, which completely blocked the waves, totally darkened the central foveal area

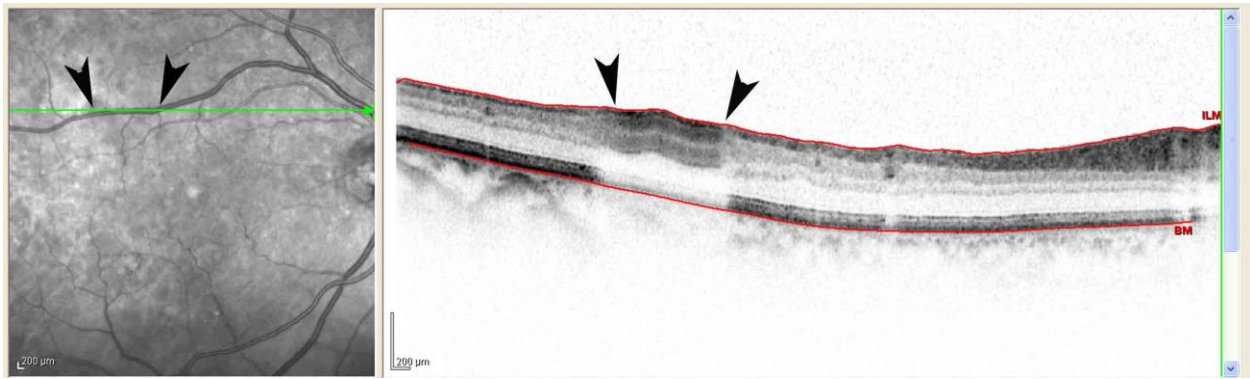


Fig.1. 31 The section of scanning laser ophthalmoscopy (SLO) optical coherence tomography crosses along the retinal large vessel (*black arrowheads*). Shadowing under large vessels is considerable and significant and sometimes creates a bizarre appearance (e.g., resembling retinal arterial occlusion). In this situation, a clinician should look at other sections and compare the location with the SLO image.

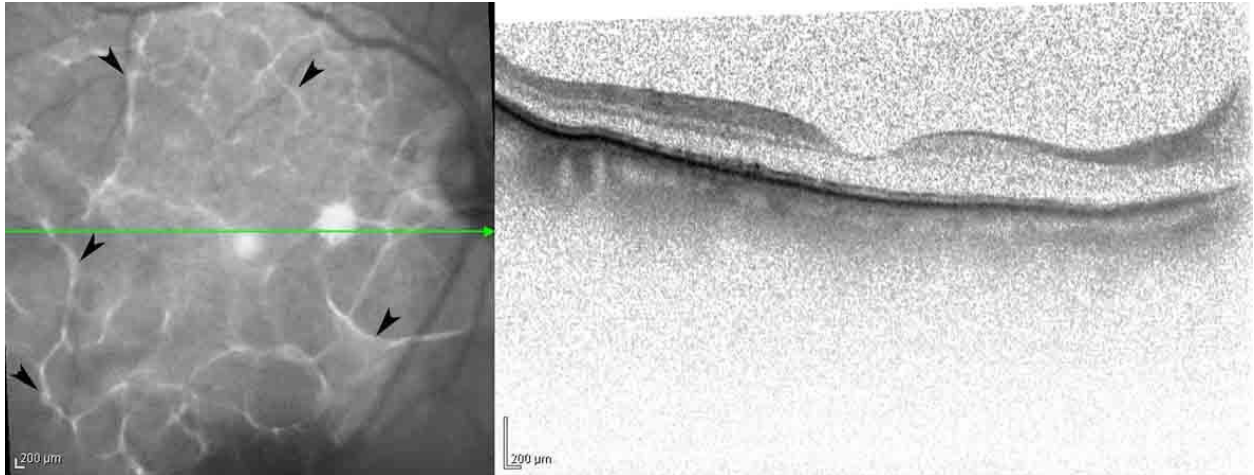


Fig.1. 32 Scanning laser ophthalmoscopy (SLO) optical coherence tomography (OCT) images of a patient with severe ocular surface disease and dry eye. Hyperreflective semicircular like lesions on the SLO image (*black arrowheads*) are diagnostic for irregular, dry ocular surface and can degrade the OCT image by scattering the laser wave light and inhibiting it from entering the posterior space

Epiretinal Membranes

By using color mode OCT, it may sometimes be difficult to identify fine epiretinal membranes(Fig.1.33). Black-in-white is more helpful for detecting thin and delicate membranes.

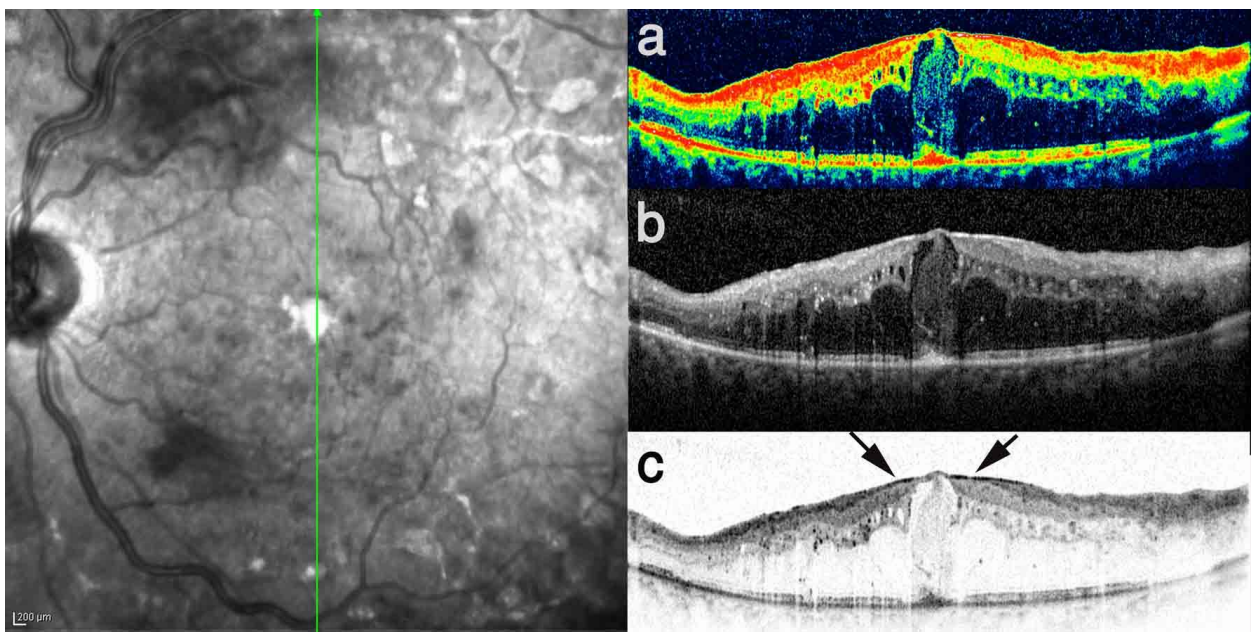


Fig.1. 33 Differences among multiple image modes in displaying the epiretinal membrane. **a** The macula in a patient with severe diabetic spongy edema is evident. The delicate epiretinal membrane covers the fovea and perifoveal area. In **b** (white-in-black mode) and **c** (black-in-white mode), the epiretinal membrane is more visible (*black arrows*)

High frequency eye movement:

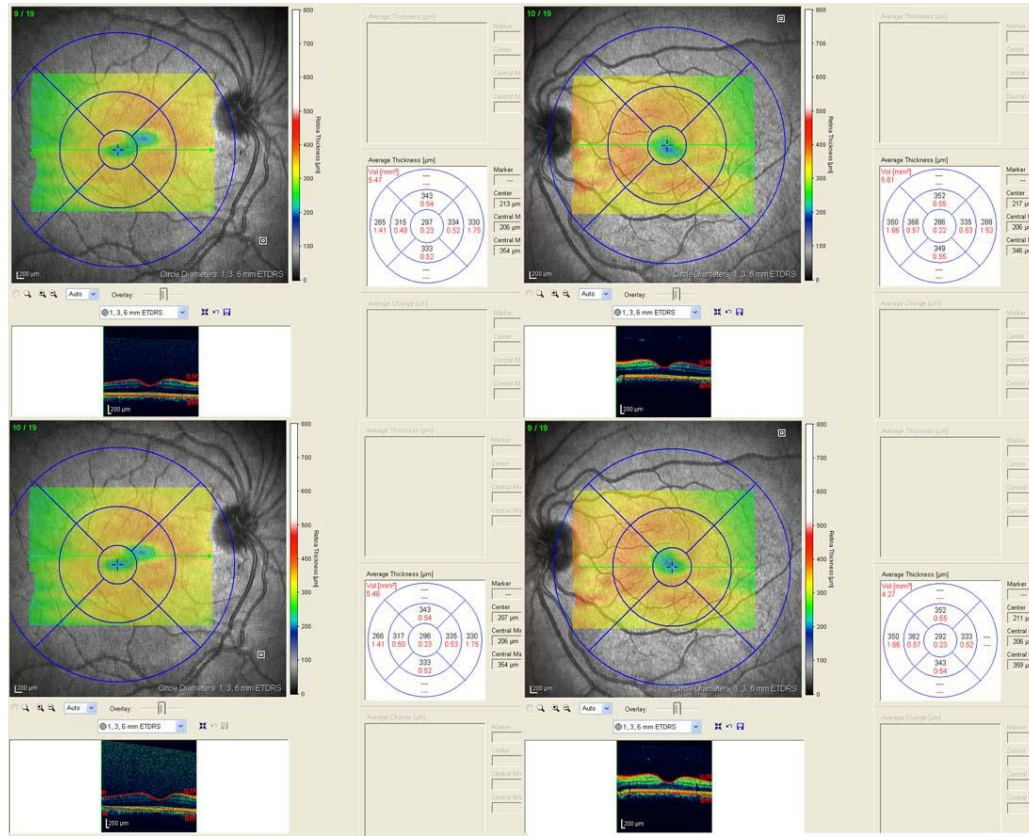


Fig.1. 34 Two foveae. The topographic maps (two different sections for each map) from a patient with high-frequency nystagmus. Despite fast acquisition of the images, two central false foveal depressions could be misidentified as the central fovea. This is an artifact that is a consequence of fast eye movement (i.e., nystagmus)

Severe ocular structure abnormality:

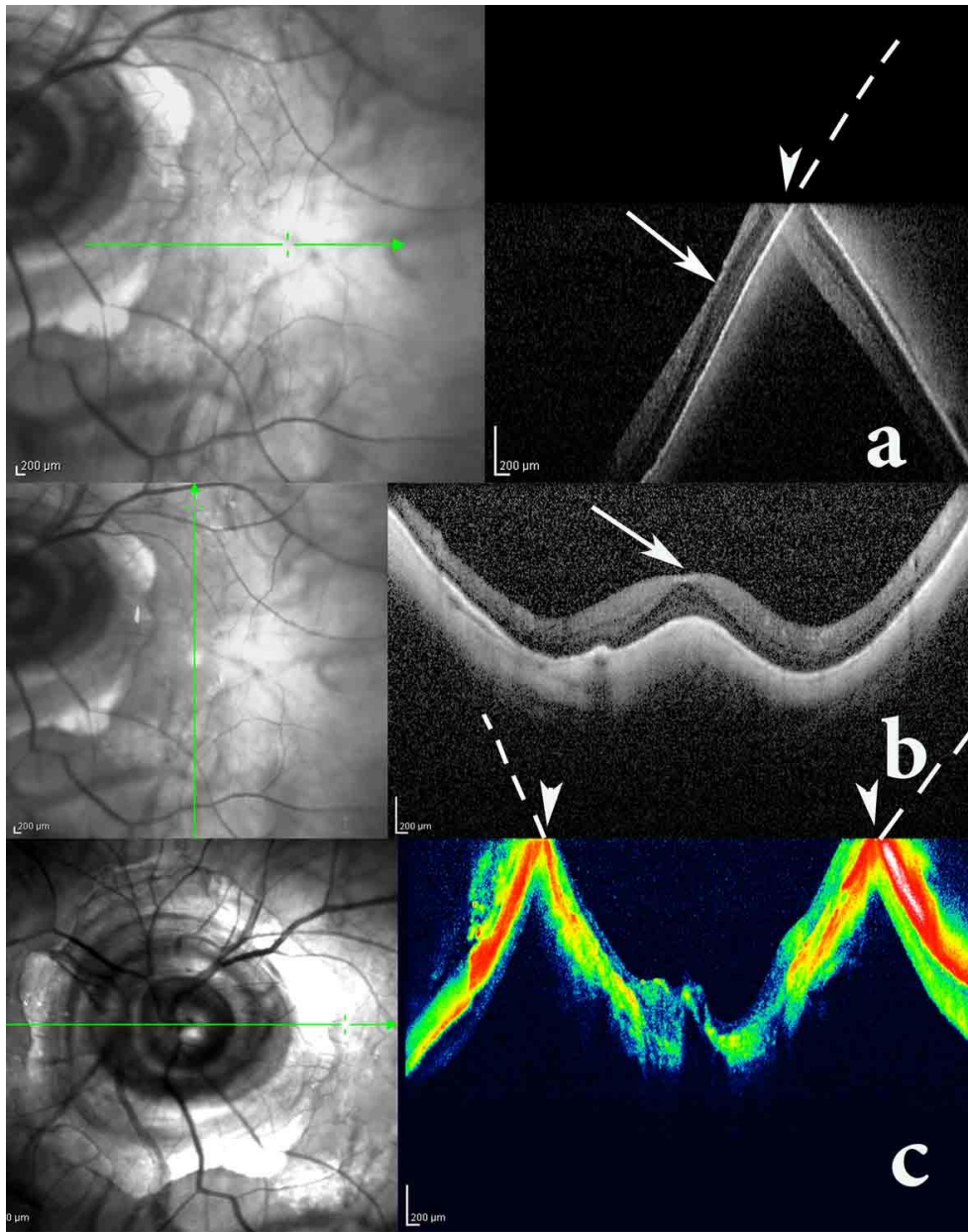


Fig.1. 35 The scanning laser ophthalmoscopy-optical coherence tomography images of a patient with myopia with a posterior staphyloma centering on the optic disc site show mirror artifacts. **a** The horizontal section presents as an oblique image because the orientation of the retinal surface with the angle of the laser-emitted light on the retina creates an inverted image (*white arrowhead with a dashed white line*) because of crossing the zero line. **b** The vertical section with a nearly vertical angle of emitted light on the retinal surface creates a more normal image, compared to the image in **a**, but without a mirror image. **c** The cross-section passes through the papillary area. The deepest part of staphyloma is at the center of the optic disc. The height of this area is more than the field of image acquisition and results in mirror artifacts. The dashed white lines indicate the actual location of the scanned site

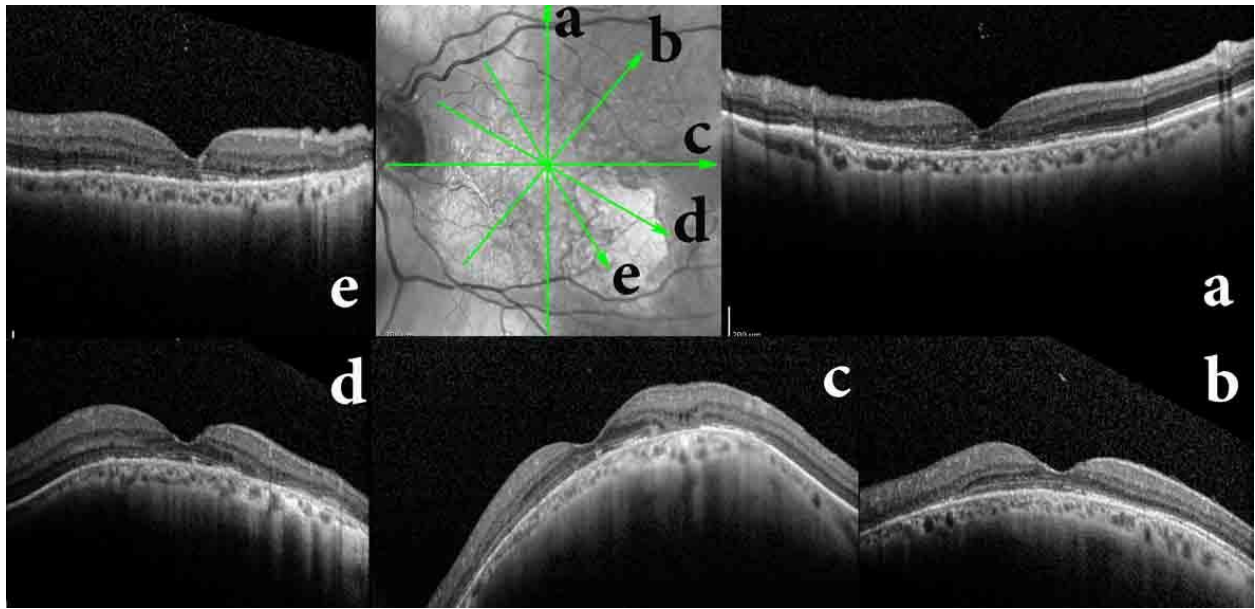


Fig.1. 36 Multiple cross-sectional images of an eye with ocular wall distortion, an elevated concave foveal area, and geographic atrophic area at the macula. On the basis of the angle of laser emission, it is possible to have multiple shapes on cross-sectional optical coherence tomography images. This factor may be a pitfall in the diagnosis and evaluation of outer retinal and choroidal lesions (e.g., choroidal masses or tumors). It can also be related to high astigmatism, which distorts the output of the laser-emitted light from the retina. This distortion could be diminished by correcting the refractive error at the beginning of the scan with the automatic compensation of distortion

Diagnostic pitfall in full thickness macular hole:

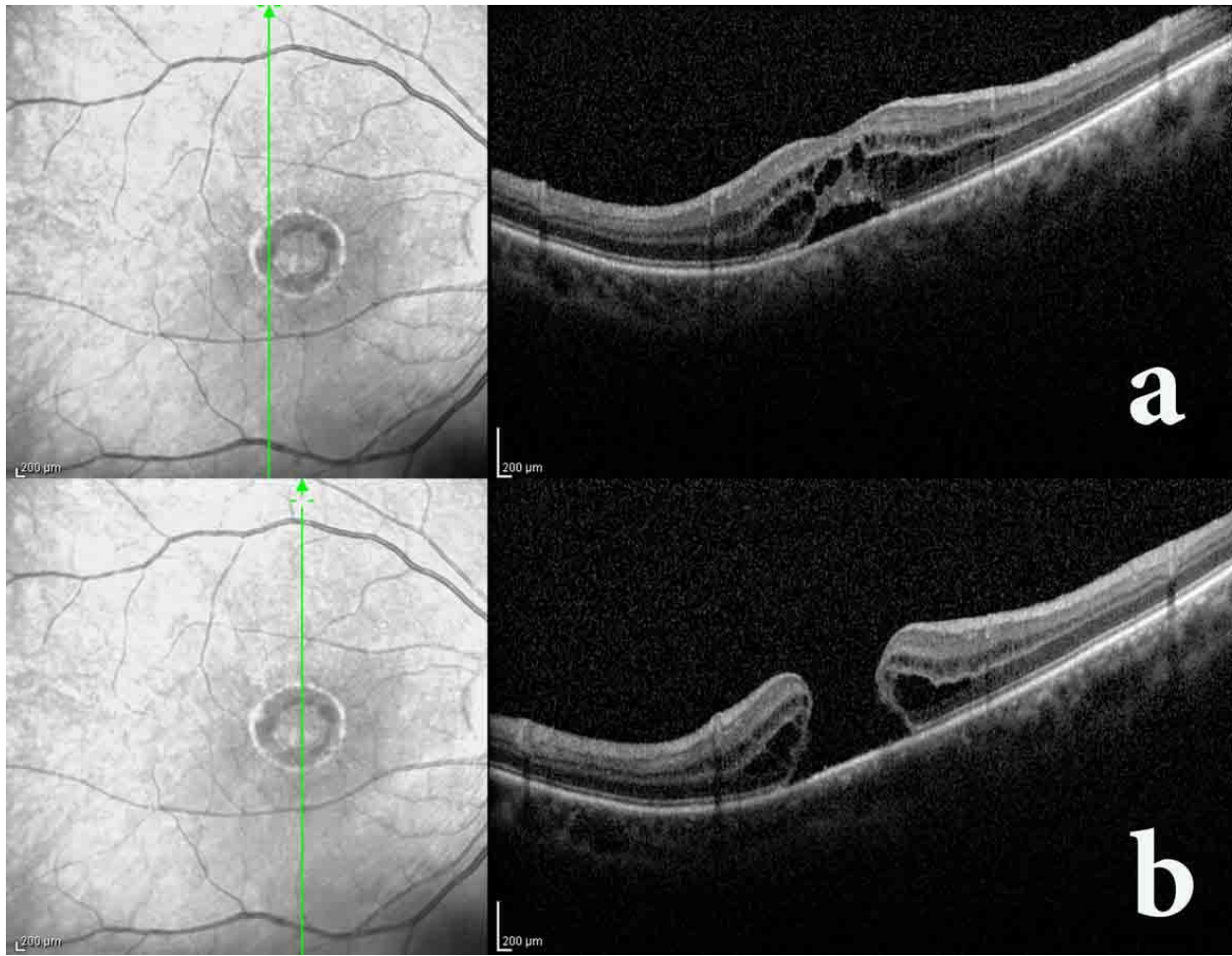


Fig.1.37 An example of a diagnostic pitfall in optical coherence tomography, especially when the scanning laser ophthalmoscopy image quality is not high. **a** On asking a patient with a full thickness macular hole because of paracentral fixation to focus on the light target of the system, the patient may focus on it with the juxtafoveal area. The consequence is exemplified in the image. This finding may be erroneously diagnosed as cystoid macular edema. **b** A scan in another area of the eye reveals full thickness discontinuity and the full thickness hole.

OCTA image artifacts

The quality of OCTA can be affected by various kinds of artifacts [80]. Any conditions such as defocusing of light beam or capacity of media can diminish the backscattering OCT signals and generate artifacts in OCTA. As a result, generated images will have low quality and produce invalid flow information. For instance, attenuation of focal OCT signals can obscure flow signal and produce shadow beneath large vessels or hyperreflective retinal lesions. Shadowing may also occur when the OCT beam cannot move through the outer retinal layers. Many pathological features reflect off light preventing it from penetration the underlying

tissues. These underlying tissues next appears as fake flow voids. SS-OCTA are more robust against this artifact than the spectral domain devices due to longer wavelength. New researches presents promising correction algorithms, which can be, incorporated in future OCTA systems.

Since OCTA reveals the motion contrast of the flowing blood, eye movements and mass tissues can induce overestimation of the flow signal and result in noise and artifacts in the achieved angiograms. To overcome this problem, motion correction methods are available in most of the commercial OCT systems. Another method is eye tracking which detects real time eye movements and correct them. Despite the corrections motion lines, duplication and discontinuity of vessels can still be observable in OCTA images.

Projection artifacts are another source of OCTA artifacts. More superficial vasculature can cause shadows on the deeper layers. This causes the pattern of superficial vascular to be duplicated on deeper layers and microcirculation. In such cases, incorrect measurements are obtained for vessel intensity in vasculature of deeper layers. These projection artifacts may even be considered as CNV by mistake. Slab subtraction and projection artifact removal (PAR) are two conventional methods for suppression of these artifacts.

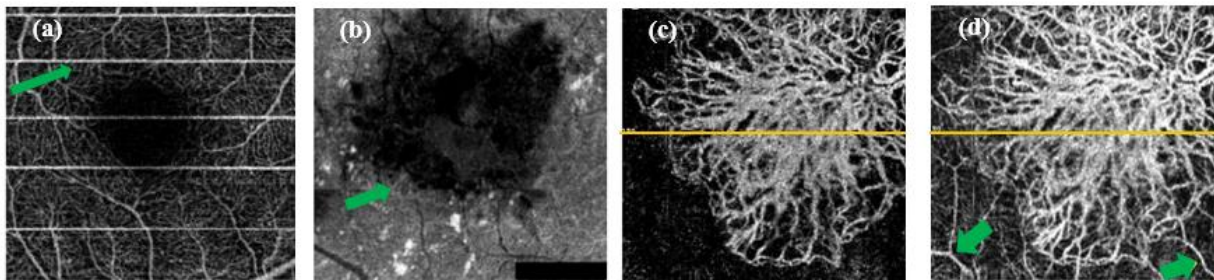


Fig.1. 38 OCTA artifacts (a) motion artifact, (b) shadowing artifact, (c), (d) projection artifact caused superficial layers visible in deeper layer (green arrows).

To produce an enface image, upper and lower boundary of 3D OCTA cube are selected and each slab is generated to project the vessels within these two boundaries. Automatic segmentation algorithms usually do this boundary selection. However, most of the segmentation algorithms are correspondent to healthy eyes with distinct retinal layers. Pathologies, such as fluid, drusens and even myopia, can change the retinal anatomy and cause mistakes in segmentation algorithms. This

leads to the segmentation artifacts in OCTA images. In such cases, manual segmentation and slab selection may help us overcome the segmentation artifacts. In slab selection, it is possible to drag a preset boundary up and down to generate larger or smaller slabs. However, manual selection allows the user to find the retinal layers manually, which is somehow time consuming. Figure 1.38 illustrates some usual artifacts in OCTA image.

VIII- Artificial intelligence in OCT image analysis

Artificial intelligence (AI), which includes machine-learning algorithms, is a computer science field trying to simulate human intelligence in computers. With growing imaging modalities such as OCT and providing a large amount of data from patients, AI programs provide computer aided diagnosis systems to analyze this vast amount of information and assist the ophthalmologists in making decisions. Machine learning programs such as support vector machines (SVM) and deep learning are trained to learn the structure of normal and abnormal data presented to them and make useful predictions for future data based on the parameters of their algorithms.

Deep learning-based algorithms usually incorporate multiple layers of interconnected networks, which is called neural network. During learning, the presented data pass through the layers allowing the program to continually learn structure of data and evaluate itself until reaching a specific performance. Unlike machine learning programs, deep learning methods do not need to explicit extraction of specific features of image data, which provides higher computational power. However, a deep learning program needs a larger training dataset than machine learning programs. Convolutional neural networks (CNN) are a powerful subset of deep learning methods [81], which are widely used in image recognition and classification, have become an inevitable part of deep learning applications in ophthalmology. Based on the configuration of the convolutional network layers and the training procedure, several task specific CNN networks have been proposed such as auto-encoders, generative adversarial networks (GAN), U-net, Res-net, Inception-net, Capsule-net, and etc. [82]. CNNs can be applied in the classification, denoising, segmentation tasks and even generating synthetic OCT data. These applications will be described briefly.

To date, several studies are done in AI and OCT imaging. Most of them focused on the image analysis of the posterior segment of the eye to interpret retinal diseases such as diabetic macular edema (DME), and AMD. Some recent studies started to investigate the performance of the AI methods in the anterior segment as well. These studies are summarized in [83].

Classification

CNNs are widely used in accurate classification of OCT images. By training the CNN using large datasets of normal and abnormal images, CNN can learn the discriminative features required for classification of data (Figure 1.39). A trained network can predict the class of unseen data accurately. Kermany et al. [84] used Inception-V3 for the classification of OCT images into four classes: choroidal neovascularization (CNV), DME, drusen, and normal and achieved the accuracy of 96.1%. Tsuji et al. [85] used a recent architecture of CNN so called Capsule-net for this four-class classification and achieved accuracy of 99.6%. In addition, they portrayed the heat map images for the respective classes to interpret the activated part of OCT image, which was used for classification (Figure 1.40).

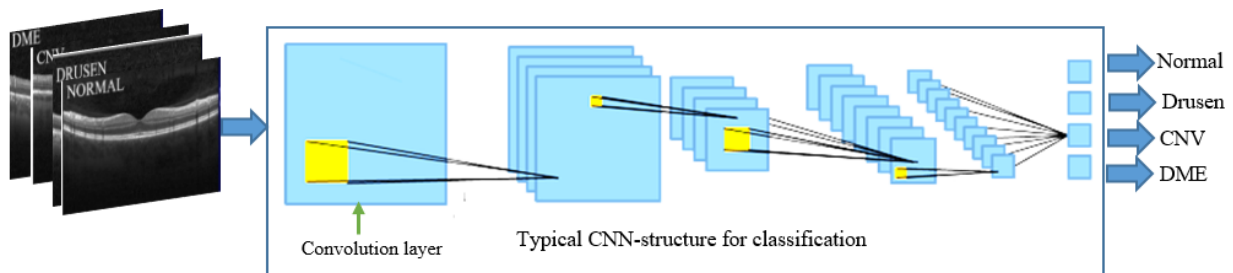


Fig.1. 39 Typical CNN structure used for classification of normal and abnormal OCT images.

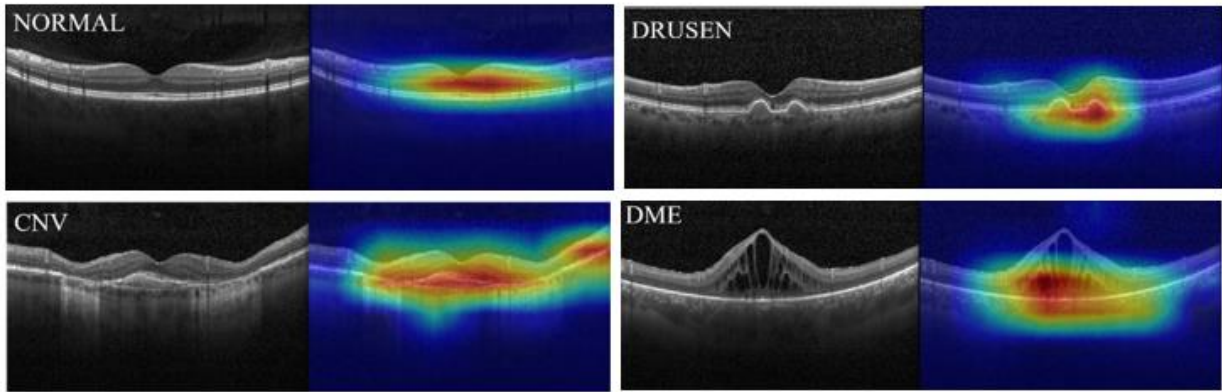


Fig.1. 40 Visualization of feature maps as heat maps after classification of four classes. Left images are input images. Right images are feature maps superimposed on an input image.

Segmentation

Deep learning methods have been applied in automatic segmentation of retinal layers, drusens, and fluids as well. The CNN structures, which are conventionally used for biomedical image segmentation, are mostly variants or extensions of U-net [86]. To train this network, which is called U-net due to its U-shape (Figure 1.41), images and their corresponding segmented images are presented to the network. After training, the network learns to produce segmented boundaries for new unseen images. Figure 1.30 illustrates the detailed structure of U-net. Several studies used modifications of U-net for OCT image segmentation. For instance, DRU-net [87] is dilated-residual U-Net deep learning network to segment optic nerve head tissues in OCT images. BAU-net [88] is also a recent boundary aware U-Net for retinal layers segmentation in OCT images.

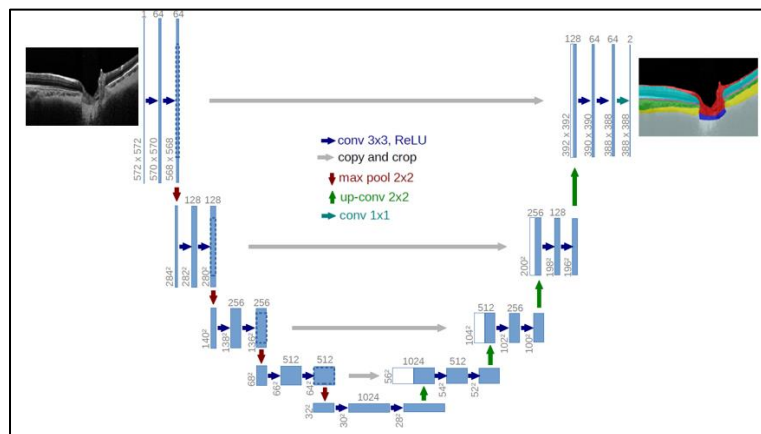


Fig.1. 41 Architecture of a traditional U-net convolutional network.

OCT image synthesis and Enhancement

Generative adversarial networks (GAN) are recent deep learning-based methods, which can be used in synthesizing the realistic OCT images. The synthetic images satisfactorily serve as the educational images for retinal specialists, and the training datasets for the classification of various retinal disorders using deep learning [89]. GAN networks consist of two neural networks that contest with each other in a game. In the training process one network, called generator, tries to produce the fake images and another network, called discriminator, tries to reveal the fake data. Given an OCT training set, the generator learns to generate new data with the same statistics as the training set.

Some OCT images have low quality and their enhancement improves clinical applications. Enhancement such as denoising [90], [91], and super-resolution [92] can also be done by GAN and auto-encoder networks.

References

- [1] J. S. Schuman, J. G. Fujimoto, C. A. Puliafito, and J. Duke, *Optical coherence tomography of ocular diseases*. Slack New Jersey:, 2004.
- [2] M. R. Hee, J. A. Izatt, E. A. Swanson, D. Huang, J. S. Schuman, C. P. Lin, C. A. Puliafito, and J. G. Fujimoto, "Optical coherence tomography of the human retina," *Arch. Ophthalmol.*, vol. 113, no. 3, pp. 325–332, 1995.
- [3] J. S. Schuman, T. Pedut-Kloizman, E. Hertzmark, M. R. Hee, J. R. Wilkins, J. G. Coker, C. A. Puliafito, J. G. Fujimoto, and E. A. Swanson, "Reproducibility of nerve fiber layer thickness measurements using optical coherence tomography," *Ophthalmology*, vol. 103, no. 11, pp. 1889–1898, 1996.
- [4] J. F. Arevalo, R. A. Garcia, J. G. Sanchez, L. Wu, D. Fuenmayor-Rivera, and A. Giral, "Angiography of Optic Nerve Diseases," in *Retinal Angiography and Optical Coherence Tomography*, Springer, 2009, pp. 155–177.
- [5] M. Leahy, J. Hogan, C. Wilson, H. Subhash, and R. Dsouza, "Multiple reference optical coherence tomography (MR-OCT) system," in *Dynamics and Fluctuations in Biomedical Photonics X*, 2013, vol. 8580, p. 85800L.
- [6] G. Song, E. T. Jelly, K. Chu, W. Y. Kendall, and A. Wax, "A review of low-cost and portable optical coherence tomography," *Prog. Biomed. Eng.*, 2021.
- [7] C. D. Lu, M. F. Kraus, B. Potsaid, J. J. Liu, W. Choi, V. Jayaraman, A. E. Cable, J. Hornegger, J. S. Duker, and J. G. Fujimoto, "Handheld ultrahigh

- speed swept source optical coherence tomography instrument using a MEMS scanning mirror,” *Biomed. Opt. Express*, vol. 5, no. 1, pp. 293–311, 2014.
- [8] W. Jung, J. Kim, M. Jeon, E. J. Chaney, C. N. Stewart, and S. A. Boppart, “Handheld optical coherence tomography scanner for primary care diagnostics,” *IEEE Trans. Biomed. Eng.*, vol. 58, no. 3, pp. 741–744, 2010.
- [9] Z. Wang, H.-C. Lee, D. Vermeulen, L. Chen, T. Nielsen, S. Y. Park, A. Ghaemi, E. Swanson, C. Doerr, and J. Fujimoto, “Silicon photonic integrated circuit swept-source optical coherence tomography receiver with dual polarization, dual balanced, in-phase and quadrature detection,” *Biomed. Opt. Express*, vol. 6, no. 7, pp. 2562–2574, 2015.
- [10] P. Pande, R. L. Shelton, G. L. Monroy, R. M. Nolan, and S. A. Boppart, “Low-cost hand-held probe for depth-resolved low-coherence interferometry,” *Biomed. Opt. Express*, vol. 8, no. 1, pp. 338–348, 2017.
- [11] J. Ho, A. C. Sull, L. N. Vuong, Y. Chen, J. Liu, J. G. Fujimoto, J. S. Schuman, and J. S. Duker, “Assessment of artifacts and reproducibility across spectral-and time-domain optical coherence tomography devices,” *Ophthalmology*, vol. 116, no. 10, pp. 1960–1970, 2009.
- [12] M. A. Sadiq, A. Rashid, R. Channa, E. Hatef, D. V Do, Q. D. Nguyen, and Y. J. Sepah, “Reliability and reproducibility of spectral and time domain optical coherence tomography images before and after correction for patients with age-related macular degeneration,” *F1000Research*, vol. 2, 2013.
- [13] S. B. Bressler, A. R. Edwards, K. V Chalam, N. M. Bressler, A. R. Glassman, G. J. Jaffe, M. Melia, D. D. Saggau, O. Z. Plous, and D. R. C. R. N. W. Committee, “Reproducibility of spectral-domain optical coherence tomography retinal thickness measurements and conversion to equivalent time-domain metrics in diabetic macular edema,” *JAMA Ophthalmol.*, vol. 132, no. 9, pp. 1113–1122, 2014.
- [14] C. A. Puliafito, M. R. Hee, C. P. Lin, E. Reichel, J. S. Schuman, J. S. Duker, J. A. Izatt, E. A. Swanson, and J. G. Fujimoto, “Imaging of macular diseases with optical coherence tomography,” *Ophthalmology*, vol. 102, no. 2, pp. 217–229, 1995.
- [15] C. C. Wykoff, A. M. Berrocal, A. C. Scheffler, S. R. Uhlhorn, M. Ruggeri, and D. Hess, “Intraoperative OCT of a full-thickness macular hole before and after internal limiting membrane peeling,” *Ophthalmic Surgery, Lasers Imaging Retin.*, vol. 41, no. 1, pp. 7–11, 2010.
- [16] C. A. Puliafito, “Optical coherence tomography: a new tool for intraoperative decision making,” *Ophthalmic Surgery, Lasers Imaging Retin.*, vol. 41, no. 1, p. 6, 2010.
- [17] R. F. Spaide and C. A. Curcio, “Anatomical correlates to the bands seen in the outer retina by optical coherence tomography: literature review and

- model,” *Retina*, vol. 31, no. 8, p. 1609, 2011.
- [18] A. J. Witkin, T. H. Ko, J. G. Fujimoto, A. Chan, W. Drexler, J. S. Schuman, E. Reichel, and J. S. Duker, “Ultra-high resolution optical coherence tomography assessment of photoreceptors in retinitis pigmentosa and related diseases,” *Am. J. Ophthalmol.*, vol. 142, no. 6, pp. 945–952, 2006.
- [19] E. T. D. R. S. R. Group, “Grading diabetic retinopathy from stereoscopic color fundus photographs—an extension of the modified Airlie House classification: ETDRS report number 10,” *Ophthalmology*, vol. 98, no. 5, pp. 786–806, 1991.
- [20] M. Wojtkowski, V. Srinivasan, J. G. Fujimoto, T. Ko, J. S. Schuman, A. Kowalczyk, and J. S. Duker, “Three-dimensional retinal imaging with high-speed ultrahigh-resolution optical coherence tomography,” *Ophthalmology*, vol. 112, no. 10, pp. 1734–1746, 2005.
- [21] V. J. Srinivasan, M. Wojtkowski, A. J. Witkin, J. S. Duker, T. H. Ko, M. Carvalho, J. S. Schuman, A. Kowalczyk, and J. G. Fujimoto, “High-definition and 3-dimensional imaging of macular pathologies with high-speed ultrahigh-resolution optical coherence tomography,” *Ophthalmology*, vol. 113, no. 11, pp. 2054–2065, 2006.
- [22] E. K. Chin, R. W. Sedek, Y. Li, L. Beckett, E. Redenbo, K. Chandra, and S. S. Park, “Reproducibility of macular thickness measurement among five OCT instruments: effects of image resolution, image registration, and eye tracking,” *Ophthalmic Surgery, Lasers Imaging Retin.*, vol. 43, no. 2, pp. 97–108, 2012.
- [23] M. Durbin, T. Abunto, M. Chang, and B. Lujan, “Retinal measurements: comparison between Cirrus HD-OCT and Stratus OCT,” *Zeiss-Meditec White Pap.*, 2009.
- [24] C. K. Leung, C. Y. Cheung, R. N. Weinreb, G. Lee, D. Lin, C. P. Pang, and D. S. C. Lam, “Comparison of macular thickness measurements between time domain and spectral domain optical coherence tomography,” *Invest. Ophthalmol. Vis. Sci.*, vol. 49, no. 11, pp. 4893–4897, 2008.
- [25] J. Huang, X. Liu, Z. Wu, H. Xiao, L. Dustin, and S. Sadda, “Macular thickness measurements in normal eyes with time domain and fourier domain optical coherence tomography,” *Retina*, vol. 29, no. 7, p. 980, 2009.
- [26] Y.-R. Roh, K. H. Park, and S. J. Woo, “Foveal thickness between stratus and spectralis optical coherence tomography in retinal diseases,” *Korean J. Ophthalmol.*, vol. 27, no. 4, pp. 268–275, 2013.
- [27] S. Grover, R. K. Murthy, V. S. Brar, and K. V Chalam, “Comparison of retinal thickness in normal eyes using Stratus and Spectralis optical coherence tomography,” *Invest. Ophthalmol. Vis. Sci.*, vol. 51, no. 5, pp. 2644–2647, 2010.

- [28] L. S. González, R. A. González, M. A. Plasencia, and P. A. Reyes, “Normal macular thickness and volume using spectral domain optical coherence tomography in a reference population,” *Arch. la Soc. Española Oftalmol. (English Ed.)*, vol. 88, no. 9, pp. 352–358, 2013.
- [29] S. H. M. Liew, C. E. Gilbert, T. D. Spector, J. Marshall, and C. J. Hammond, “The role of heredity in determining central retinal thickness,” *Br. J. Ophthalmol.*, vol. 91, no. 9, pp. 1143–1147, 2007.
- [30] U. Eriksson and A. Alm, “Macular thickness decreases with age in normal eyes: a study on the macular thickness map protocol in the Stratus OCT,” *Br. J. Ophthalmol.*, vol. 93, no. 11, pp. 1448–1452, 2009.
- [31] J. A. Izatt, M. R. Hee, E. A. Swanson, C. P. Lin, D. Huang, J. S. Schuman, C. A. Puliafito, and J. G. Fujimoto, “Micrometer-scale resolution imaging of the anterior eye in vivo with optical coherence tomography,” *Arch. Ophthalmol.*, vol. 112, no. 12, pp. 1584–1589, 1994.
- [32] R. F. Steinert and D. Huang, *Anterior segment optical coherence tomography*. Slack Incorporated, 2008.
- [33] J. Shan, C. DeBoer, and B. Y. Xu, “Anterior segment optical coherence tomography: applications for clinical care and scientific research,” *Asia-Pacific J. Ophthalmol. (Philadelphia, Pa.)*, 2019.
- [34] S. Siebelmann, P. Scholz, S. Sonnenschein, B. Bachmann, M. Matthaei, C. Cursiefen, and L. M. Heindl, “Anterior segment optical coherence tomography for the diagnosis of corneal dystrophies according to the IC3D classification,” *Surv. Ophthalmol.*, vol. 63, no. 3, pp. 365–380, 2018.
- [35] M. Kim, S. S. Kim, H. J. Kwon, H. J. Koh, and S. C. Lee, “Association between choroidal thickness and ocular perfusion pressure in young, healthy subjects: enhanced depth imaging optical coherence tomography study,” *Invest. Ophthalmol. Vis. Sci.*, vol. 53, no. 12, pp. 7710–7717, 2012.
- [36] Y. Ikuno, I. Maruko, Y. Yasuno, M. Miura, T. Sekiryu, K. Nishida, and T. Iida, “Reproducibility of retinal and choroidal thickness measurements in enhanced depth imaging and high-penetration optical coherence tomography,” *Invest. Ophthalmol. Vis. Sci.*, vol. 52, no. 8, pp. 5536–5540, 2011.
- [37] R. Margolis and R. F. Spaide, “A pilot study of enhanced depth imaging optical coherence tomography of the choroid in normal eyes,” *Am. J. Ophthalmol.*, vol. 147, no. 5, pp. 811–815, 2009.
- [38] V. Manjunath, M. Taha, J. G. Fujimoto, and J. S. Duker, “Choroidal thickness in normal eyes measured using Cirrus HD optical coherence tomography,” *Am. J. Ophthalmol.*, vol. 150, no. 3, pp. 325–329, 2010.
- [39] T. Agawa, M. Miura, Y. Ikuno, S. Makita, T. Fabritius, T. Iwasaki, H. Goto, K. Nishida, and Y. Yasuno, “Choroidal thickness measurement in healthy

- Japanese subjects by three-dimensional high-penetration optical coherence tomography,” *Graefe’s Arch. Clin. Exp. Ophthalmol.*, vol. 249, no. 10, pp. 1485–1492, 2011.
- [40] M. Hirata, A. Tsujikawa, A. Matsumoto, M. Hangai, S. Ooto, K. Yamashiro, M. Akiba, and N. Yoshimura, “Macular choroidal thickness and volume in normal subjects measured by swept-source optical coherence tomography,” *Invest. Ophthalmol. Vis. Sci.*, vol. 52, no. 8, pp. 4971–4978, 2011.
- [41] M. Esmaelpour, B. Považay, B. Hermann, B. Hofer, V. Kajić, K. Kapoor, N. J. L. Sheen, R. V North, and W. Drexler, “Three-dimensional 1060-nm OCT: choroidal thickness maps in normal subjects and improved posterior segment visualization in cataract patients,” *Invest. Ophthalmol. Vis. Sci.*, vol. 51, no. 10, pp. 5260–5266, 2010.
- [42] V. Manjunath, J. Goren, J. G. Fujimoto, and J. S. Duker, “Analysis of choroidal thickness in age-related macular degeneration using spectral-domain optical coherence tomography,” *Am. J. Ophthalmol.*, vol. 152, no. 4, pp. 663–668, 2011.
- [43] R. F. Spaide, “Age-related choroidal atrophy,” *Am. J. Ophthalmol.*, vol. 147, no. 5, pp. 801–810, 2009.
- [44] G. Querques, L. Querques, R. Forte, N. Massamba, F. Coscas, and E. H. Souied, “Choroidal changes associated with reticular pseudodrusen,” *Invest. Ophthalmol. Vis. Sci.*, vol. 53, no. 3, pp. 1258–1263, 2012.
- [45] P. Rishi, E. Rishi, G. Mathur, and V. Raval, “Ocular perfusion pressure and choroidal thickness in eyes with polypoidal choroidal vasculopathy, wet-age-related macular degeneration, and normals,” *Eye*, vol. 27, no. 9, pp. 1038–1043, 2013.
- [46] P. Jirarattanasopa, S. Ooto, I. Nakata, A. Tsujikawa, K. Yamashiro, A. Oishi, and N. Yoshimura, “Choroidal thickness, vascular hyperpermeability, and complement factor H in age-related macular degeneration and polypoidal choroidal vasculopathy,” *Invest. Ophthalmol. Vis. Sci.*, vol. 53, no. 7, pp. 3663–3672, 2012.
- [47] J. T. Kim, D. H. Lee, S. G. Joe, J.-G. Kim, and Y. H. Yoon, “Changes in choroidal thickness in relation to the severity of retinopathy and macular edema in type 2 diabetic patients,” *Invest. Ophthalmol. Vis. Sci.*, vol. 54, no. 5, pp. 3378–3384, 2013.
- [48] G. Querques, R. Lattanzio, L. Querques, C. Del Turco, R. Forte, L. Pierro, E. H. Souied, and F. Bandello, “Enhanced depth imaging optical coherence tomography in type 2 diabetes,” *Invest. Ophthalmol. Vis. Sci.*, vol. 53, no. 10, pp. 6017–6024, 2012.
- [49] M. Gemenetzi, G. De Salvo, and A. J. Lotery, “Central serous chorioretinopathy: an update on pathogenesis and treatment,” *Eye*, vol. 24,

- no. 12, pp. 1743–1756, 2010.
- [50] Y. Imamura, T. Fujiwara, R. O. N. Margolis, and R. F. Spaide, “Enhanced depth imaging optical coherence tomography of the choroid in central serous chorioretinopathy,” *Retina*, vol. 29, no. 10, pp. 1469–1473, 2009.
- [51] V. Manjunath, J. G. Fujimoto, and J. S. Duker, “Cirrus HD-OCT high definition imaging is another tool available for visualization of the choroid and provides agreement with the finding that the choroidal thickness is increased in central serous chorioretinopathy in comparison to normal eyes.,” *Retina*, vol. 30, no. 8, pp. 1320–1321, 2010.
- [52] S.-W. Kim, J. Oh, S.-S. Kwon, J. Yoo, and K. Huh, “Comparison of choroidal thickness among patients with healthy eyes, early age-related maculopathy, neovascular age-related macular degeneration, central serous chorioretinopathy, and polypoidal choroidal vasculopathy,” *Retina*, vol. 31, no. 9, pp. 1904–1911, 2011.
- [53] L. Yang, J. B. Jonas, and W. Wei, “Optical coherence tomography–assisted enhanced depth imaging of central serous chorioretinopathy,” *Invest. Ophthalmol. Vis. Sci.*, vol. 54, no. 7, pp. 4659–4665, 2013.
- [54] R. L. Furlanetto, S. C. Park, U. J. Damle, S. F. Sieminski, Y. Kung, N. Siegal, J. M. Liebmann, and R. Ritch, “Posterior displacement of the lamina cribrosa in glaucoma: in vivo interindividual and intereye comparisons,” *Invest. Ophthalmol. Vis. Sci.*, vol. 54, no. 7, pp. 4836–4842, 2013.
- [55] S. Kiumehr, S. C. Park, S. Dorairaj, C. C. Teng, C. Tello, J. M. Liebmann, and R. Ritch, “In vivo evaluation of focal lamina cribrosa defects in glaucoma,” *Arch. Ophthalmol.*, vol. 130, no. 5, pp. 552–559, 2012.
- [56] S. C. Park, C. G. V De Moraes, C. C. Teng, C. Tello, J. M. Liebmann, and R. Ritch, “Enhanced depth imaging optical coherence tomography of deep optic nerve complex structures in glaucoma,” *Ophthalmology*, vol. 119, no. 1, pp. 3–9, 2012.
- [57] I. Maruko, T. Iida, Y. Sugano, H. Oyamada, T. Sekiryu, T. Fujiwara, and R. F. Spaide, “Subfoveal choroidal thickness after treatment of Vogt–Koyanagi–Harada disease,” *Retina*, vol. 31, no. 3, pp. 510–517, 2011.
- [58] M. Nakayama, H. Keino, A. A. Okada, T. Watanabe, W. Taki, M. Inoue, and A. Hirakata, “Enhanced depth imaging optical coherence tomography of the choroid in Vogt–Koyanagi–Harada disease,” *Retina*, vol. 32, no. 10, pp. 2061–2069, 2012.
- [59] A. H. C. Fong, K. K. W. Li, and D. Wong, “Choroidal evaluation using enhanced depth imaging spectral-domain optical coherence tomography in Vogt–Koyanagi–Harada disease,” *Retina*, vol. 31, no. 3, pp. 502–509, 2011.
- [60] F. T. da Silva, V. M. Sakata, A. Nakashima, C. E. Hirata, E. Olivalves, W. Y. Takahashi, R. A. Costa, and J. H. Yamamoto, “Enhanced depth imaging

- optical coherence tomography in long-standing Vogt–Koyanagi–Harada disease,” *Br. J. Ophthalmol.*, vol. 97, no. 1, pp. 70–74, 2013.
- [61] Y. Yasuno, F. Okamoto, K. Kawana, T. Yatagai, and T. Oshika, “Investigation of multifocal choroiditis with panuveitis by three-dimensional high-penetration optical coherence tomography,” *J. Biophotonics*, vol. 2, no. 6-7, pp. 435–441, 2009.
- [62] T. Fujiwara, Y. Imamura, R. Margolis, J. S. Slakter, and R. F. Spaide, “Enhanced depth imaging optical coherence tomography of the choroid in highly myopic eyes,” *Am. J. Ophthalmol.*, vol. 148, no. 3, pp. 445–450, 2009.
- [63] M. Hayashi, Y. Ito, A. Takahashi, K. Kawano, and H. Terasaki, “Scleral thickness in highly myopic eyes measured by enhanced depth imaging optical coherence tomography,” *Eye*, vol. 27, no. 3, pp. 410–417, 2013.
- [64] Y. Imamura, T. Iida, I. Maruko, S. A. Zweifel, and R. F. Spaide, “Enhanced depth imaging optical coherence tomography of the sclera in dome-shaped macula,” *Am. J. Ophthalmol.*, vol. 151, no. 2, pp. 297–302, 2011.
- [65] R. F. Spaide, J. G. Fujimoto, N. K. Waheed, S. R. Sadda, and G. Staurenghi, “Optical coherence tomography angiography,” *Prog. Retin. Eye Res.*, vol. 64, pp. 1–55, 2018.
- [66] J. Fingler, C. Readhead, D. M. Schwartz, and S. E. Fraser, “Phase-contrast OCT imaging of transverse flows in the mouse retina and choroid,” *Invest. Ophthalmol. Vis. Sci.*, vol. 49, no. 11, pp. 5055–5059, 2008.
- [67] X.-X. Li, W. Wu, H. Zhou, J.-J. Deng, M.-Y. Zhao, T.-W. Qian, C. Yan, X. Xu, and S.-Q. Yu, “A quantitative comparison of five optical coherence tomography angiography systems in clinical performance,” *Int. J. Ophthalmol.*, vol. 11, no. 11, p. 1784, 2018.
- [68] R. Told, S. Sacu, A. Hecht, M. Baratsits, K. Eibenberger, M. E. Kroh, S. Rezar-Dreindl, F. G. Schlanitz, G. Weigert, and A. Pollreisz, “Comparison of SD-optical coherence tomography angiography and indocyanine green angiography in type 1 and 2 neovascular age-related macular degeneration,” *Invest. Ophthalmol. Vis. Sci.*, vol. 59, no. 6, pp. 2393–2400, 2018.
- [69] A. Y. Alibhai, E. M. Moulton, R. Shahzad, C. B. Rebhun, C. Moreira-Neto, M. McGowan, D. Lee, B. Lee, C. R. Baumal, and A. J. Witkin, “Quantifying microvascular changes using OCT angiography in diabetic eyes without clinical evidence of retinopathy,” *Ophthalmol. Retin.*, vol. 2, no. 5, pp. 418–427, 2018.
- [70] N. Takase, M. Nozaki, A. Kato, H. Ozeki, M. Yoshida, and Y. Ogura, “Enlargement of foveal avascular zone in diabetic eyes evaluated by en face optical coherence tomography angiography,” *Retina*, vol. 35, no. 11, pp. 2377–2383, 2015.
- [71] A. Ishibazawa, T. Nagaoka, A. Takahashi, T. Omae, T. Tani, K. Sogawa, H.

- Yokota, and A. Yoshida, "Optical coherence tomography angiography in diabetic retinopathy: a prospective pilot study," *Am. J. Ophthalmol.*, vol. 160, no. 1, pp. 35–44, 2015.
- [72] D. Gildea, "The diagnostic value of optical coherence tomography angiography in diabetic retinopathy: a systematic review," *Int. Ophthalmol.*, vol. 39, no. 10, pp. 2413–2433, 2019.
- [73] N. K. Waheed, E. M. Moulton, J. G. Fujimoto, and P. J. Rosenfeld, "Optical coherence tomography angiography of dry age-related macular degeneration," *OCT Angiogr. Retin. Macular Dis.*, vol. 56, pp. 91–100, 2016.
- [74] L. Roisman and R. Goldhardt, "OCT Angiography: an upcoming non-invasive tool for diagnosis of age-related macular degeneration," *Curr. Ophthalmol. Rep.*, vol. 5, no. 2, pp. 136–140, 2017.
- [75] H. Akil, A. S. Huang, B. A. Francis, S. R. Sadda, and V. Chopra, "Retinal vessel density from optical coherence tomography angiography to differentiate early glaucoma, pre-perimetric glaucoma and normal eyes," *PLoS One*, vol. 12, no. 2, p. e0170476, 2017.
- [76] R. Ray, S. S. Stinnett, and G. J. Jaffe, "Evaluation of image artifact produced by optical coherence tomography of retinal pathology," *Am. J. Ophthalmol.*, vol. 139, no. 1, pp. 18–29, 2005.
- [77] J. Ho, D. P. E. Castro, L. C. Castro, Y. Chen, J. Liu, C. Mattox, C. Krishnan, J. G. Fujimoto, J. S. Schuman, and J. S. Duker, "Clinical assessment of mirror artifacts in spectral-domain optical coherence tomography," *Invest. Ophthalmol. Vis. Sci.*, vol. 51, no. 7, pp. 3714–3720, 2010.
- [78] S. M. Waldstein, B. S. Gerendas, A. Montuoro, C. Simader, and U. Schmidt-Erfurth, "Quantitative comparison of macular segmentation performance using identical retinal regions across multiple spectral-domain optical coherence tomography instruments," *Br. J. Ophthalmol.*, vol. 99, no. 6, pp. 794–800, 2015.
- [79] E. Z. Karam, E. Ramirez, P. L. Arreaza, and J. Morales-Stopello, "Optical coherence tomographic artefacts in diseases of the retinal pigment epithelium," *Br. J. Ophthalmol.*, vol. 91, no. 9, pp. 1139–1142, 2007.
- [80] C. Enders, G. E. Lang, J. Dreyhaupt, M. Loidl, G. K. Lang, and J. U. Werner, "Quantity and quality of image artifacts in optical coherence tomography angiography," *PLoS One*, vol. 14, no. 1, p. e0210505, 2019.
- [81] L. Lu, X. Wang, G. Carneiro, and L. Yang, *Deep learning and convolutional neural networks for medical imaging and clinical informatics*. Springer, 2019.
- [82] A. Khan, A. Sohail, U. Zahoora, and A. S. Qureshi, "A survey of the recent architectures of deep convolutional neural networks," *Artif. Intell. Rev.*, vol. 53, no. 8, pp. 5455–5516, 2020.

- [83] R. Kapoor, B. T. Whigham, and L. A. Al-Aswad, "Artificial intelligence and optical coherence tomography imaging," *Asia-Pacific J. Ophthalmol.*, vol. 8, no. 2, pp. 187–194, 2019.
- [84] D. S. Kermany, M. Goldbaum, W. Cai, C. C. S. Valentim, H. Liang, S. L. Baxter, A. McKeown, G. Yang, X. Wu, and F. Yan, "Identifying medical diagnoses and treatable diseases by image-based deep learning," *Cell*, vol. 172, no. 5, pp. 1122–1131, 2018.
- [85] T. Tsuji, Y. Hirose, K. Fujimori, T. Hirose, A. Oyama, Y. Saikawa, T. Mimura, K. Shiraishi, T. Kobayashi, and A. Mizota, "Classification of optical coherence tomography images using a capsule network," *BMC Ophthalmol.*, vol. 20, no. 1, pp. 1–9, 2020.
- [86] O. Ronneberger, P. Fischer, and T. Brox, "U-net: Convolutional networks for biomedical image segmentation," in *International Conference on Medical image computing and computer-assisted intervention*, 2015, pp. 234–241.
- [87] S. K. Devalla, P. K. Renukanand, B. K. Sreedhar, G. Subramanian, L. Zhang, S. Perera, J.-M. Mari, K. S. Chin, T. A. Tun, and N. G. Strouthidis, "DRUNET: a dilated-residual U-Net deep learning network to segment optic nerve head tissues in optical coherence tomography images," *Biomed. Opt. Express*, vol. 9, no. 7, pp. 3244–3265, 2018.
- [88] B. Wang, W. Wei, S. Qiu, S. Wang, D. Li, and H. He, "Boundary Aware U-Net for Retinal Layers Segmentation in Optical Coherence Tomography Images," *IEEE J. Biomed. Heal. Informatics*, 2021.
- [89] C. Zheng, X. Xie, K. Zhou, B. Chen, J. Chen, H. Ye, W. Li, T. Qiao, S. Gao, and J. Yang, "Assessment of generative adversarial networks model for synthetic optical coherence tomography images of retinal disorders," *Transl. Vis. Sci. Technol.*, vol. 9, no. 2, p. 29, 2020.
- [90] M. Tajmiriahi, R. Kafieh, Z. Amini, and H. Rabbani, "A Lightweight Mimic Convolutional Auto-encoder for Denoising Retinal Optical Coherence Tomography Images," *IEEE Trans. Instrum. Meas.*, 2021.
- [91] A. Guo, L. Fang, M. Qi, and S. Li, "Unsupervised Denoising of Optical Coherence Tomography Images with Nonlocal-Generative Adversarial Network," *IEEE Trans. Instrum. Meas.*, 2020.
- [92] V. Das, S. Dandapat, and P. K. Bora, "Unsupervised super-resolution of OCT images using generative adversarial network for improved age-related macular degeneration diagnosis," *IEEE Sens. J.*, vol. 20, no. 15, pp. 8746–8756, 2020.